Journal of
Manufacturing and Materials Processing

MDPI

Review

A Review of the Recent Developments and Challenges in Wire Arc Additive Manufacturing (WAAM) Process

Abid Shah *, Rezo Aliyev, Henning Zeidler and Stefan Krinke

Institute for Machine Elements, Engineering Design and Manufacturing (IMKF), Technische Universität Bergakademie Freiberg, Agricolastr. 1, 09599 Freiberg, Germany
* Correspondence: abid.shah@doktorand.tu-freiberg.de

Abstract: Wire arc additive manufacturing (WAAM) is an emerging and promising technology for producing medium-to-large-scale metallic components/structures for different industries, i.e., aerospace, automotive, shipbuilding, etc. It is now a feasible alternative to traditional manufacturing processes due to its shorter lead time, low material waste, and cost-effectiveness. WAAM has been widely used to produce components using different materials, including copper-based alloy wires, in the past decades. This review paper highlights the critical aspects of WAAM process in terms of technology, various challenges faced during WAAM process, different in-process and post-process operations, process monitoring methods, various gases, and different types of materials used in WAAM process. Furthermore, it briefly overviews recent developments in depositing different copper-based alloys via WAAM process.

Keywords: WAAM; copper-based alloys; CMT; 3D printing; directed energy deposition; material deposition; monitoring; in-process operations; post-process operations

check for updates

Citation: Shah, A.; Aliyev, R.; Zeidler, H.; Krinke, S. A Review of the Recent Developments and Challenges in Wire Arc Additive Manufacturing (WAAM) Process. *J. Manuf. Mater. Process.* **2023**, *7*, 97. https://doi.org/10.3390/jmmp7030097

Academic Editor: Yu-Ming Zhang

Received: 4 April 2023
Revised: 28 April 2023
Accepted: 8 May 2023
Published: 14 May 2023

Correction Statement: This article has been republished with a minor change. The change does not affect the scientific content of the article and further details are available within the backmatter of the website version of this article.

Copyright: © 2023 by the authors. Licensee MDPI, Basel, Switzerland. This article is an open access article distributed under the terms and conditions of the Creative Commons Attribution (CC BY) license (https://creativecommons.org/licenses/by/4.0/).

1. Introduction

Additive manufacturing (AM), commonly known as 3D printing [1], is the technology used to manufacture parts and objects through layer-by-layer deposition of materials. AM is considered one of the most innovative manufacturing technologies of the 21st century. It integrates the leading world technologies, e.g., digital modeling, machining, material processing, and metallurgical engineering. According to ISO/ASTM 52900:2021, AM processes can be divided into the following categories, as shown in Figure 1.

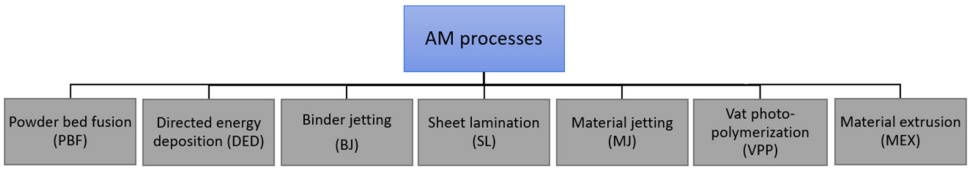

Figure 1. AM types.

AM offers significant benefits in reducing cycle time and saving raw materials by depositing material layer-by-layer under computer control. Especially, it can generate complicated geometrical features in the parts with high precision and lower dependency on cutting tools, dies, fixtures, and other complex machining processes [2,3].

Powder bed fusion (PBF) and directed energy deposition (DED) have recently attracted more attention among all available AM technologies. Although PBF can produce parts with complex geometries and high accuracy, it also has some drawbacks, including high costs (operational cost, equipment cost, material cost) and the use of metal powder, which can be very unhealthy for humans. Furthermore, a controlled environment is needed where the PBF process takes place to prevent people from inhaling the toxic powder. DED is a

promising method for AM of metals to overcome the aforementioned issues. DED is an AM methodology in which focused thermal energy is utilized to melt the material as it is deposited. In DED, the wire or powder material is used as feedstock and a heat source (plasma, electric arc, laser, or electron beam) for material deposition on a substrate surface. Although there is a lower resolution in DED compared to PBF, the material deposition rate is much higher in DED. However, some studies of AM technologies also reported a few drawbacks to DED-based AM methods. These drawbacks include the utilization of large volumes of inert gases in laser-based DED, the high vacuum required in electron-based DED, etc. Furthermore, powder-based DED has lower material deposition efficiency than wire-based DED, as a minor portion of the total powder will not be melted. That is why if the wire is used as a feedstock in DED instead of metal powder, it omits the need for recycling and powder protection systems, and the cost of raw materials is reduced significantly. A comparison of different AM processes is presented below in Table 1.

Table 1. Comparison of AM processes [4–8].

AM Type	Sub-Types/Techniques	Binding Mechanism	Feedstock	Activation Source
Powder bed fusion (PBF)	Direct metal laser sintering Selective laser sintering Electron beam melting Selective laser melting	Thermal reaction	Powder	Thermal energy in the form of laser, infrared light, or electron beam
Directed energy deposition (DED)	Laser-engineered net shaping Electron beam freeform fabrication Laser consolidation Wire arc additive manufacturing (WAAM) Directed light fabrication	Thermal reaction	Powder or wire	Laser, arc or plasma beam, electron beam
Binder jetting (BJ)		Chemical or thermal reaction	Liquid binder or powder	Liquid binder
Sheet lamination (SL)	Ultrasonic consolidation Laminated object manufacturing	Ultrasonic connection or thermal or chemical reaction	Sheet	Thermal, chemical reaction, or ultrasonic transducer
Material jetting (MJ)		Curing or chemical reaction	Molten wax or liquid-photosensitive resin	Temperature field or radiation source
Material extrusion (MEX)		Chemical or thermal reaction	Wire or paste	Ultrasonic, heat, or chemical reaction
Vat photo-polymerization (VPP)	Stereolithography (SLA) Digital Light Processing (DLP) Continuous Digital Light Processing/Continuous Liquid Interface Production (CDLP/CLIP)	Chemical reaction curing	Photosensitive resin	Ultraviolet light

2. WAAM Process

2.1. Introduction to WAAM

The wire arc additive manufacturing (WAAM) process has become a renowned AM process in the recent decade, and it is one of the DED technologies. WAAM has been derived from classical arc welding technology [9–11]. In WAAM process, the wire is melted through heating by using an electric arc and then transferred to the molten metal pool. Later, it solidifies at the melt pool boundary and produces the part layer-by-layer [12]. A typical WAAM process is shown in Figure 2 below.

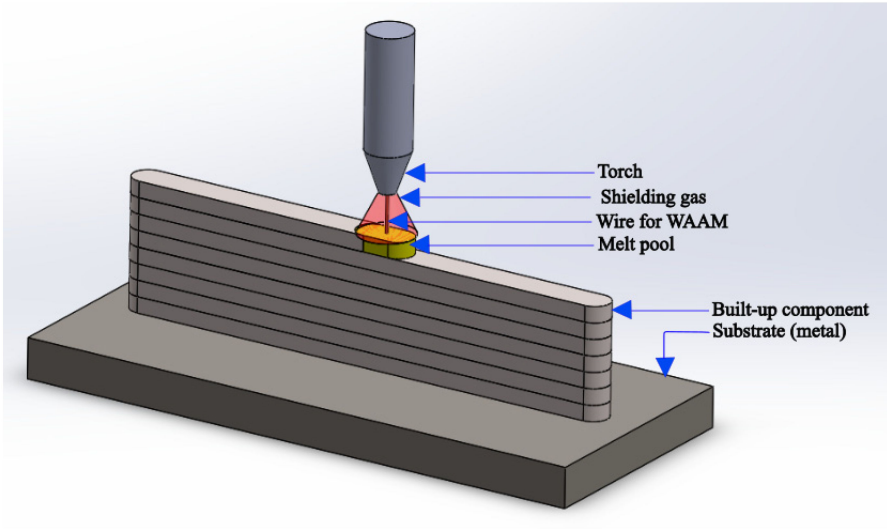

Figure 2. WAAM process.

WAAM process has the potential to develop structures that can be extended to tens of meters and can fabricate fully dense parts with large dimensions, along with higher manufacturing efficiency and low production costs. It is also suitable for repairing and maintaining damaged parts and components. Generally, the direct cost of metal wire used in WAAM process is roughly 10% of the metal powder having the same weight [12]. A comparison of the material deposition rate in WAAM process with other AM processes is presented below in Table 2.

Table 2. Comparison of material deposition rates of major AM processes for steels [13,14].

Type of AM Process	SLM Process	EBM Process	LMD Process	WAAM Process
Material deposition rate (g/h)	40–100	100–300	150–2400	500–10,000

WAAM process can be divided into three major categories depending on the type of arc-based welding technology used to melt the feed wire and generate a 3D object/structure layer by layer [15–18]. These three different types include gas tungsten arc welding (GTAW), plasma arc welding (PAW), and gas metal arc welding (GMAW), as shown in Figure 3.

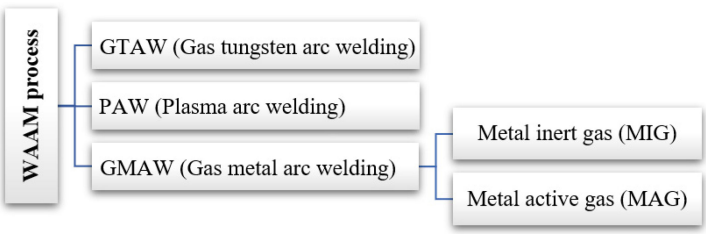

Figure 3. Types of WAAM process.

In GTAW-based WAAM, an electric arc is generated between a non-consumable tungsten electrode and the substrate material for heat generation, as shown in Figure 4a below. A filler wire is fed from the side, which melts due to the arc's heat and deposits on the substrate's surface to get the desired geometry (width, height, cross-section, etc.) and mechanical properties. The PAW process is similar to GTAW in that a non-consumable electrode is used in both methods. However, PAW differs from GTAW in welding torch construction and is more efficient than GTAW because the plasma arc is constricted in a nozzle. In PAW, an arc is generated between the tungsten electrode and the water-cooled

nozzle, as shown below in Figure 4b. The inert gas flowing through the arcing zone of the torch gets ionized, i.e., the gas turns into a plasma state. This plasma jet is then transferred through a small orifice to the substrate. This plasma jet turns the filler wire into molten form due to the high heat. In addition, shielding gas is used to protect the molten pool from contamination. But the initial cost of PAW is very high compared to GMAW and GTAW. GMAW is widely used for WAAM process nowadays compared to other WAAM processes due to its higher material deposition rate, high material utilization, and shorter lead time. In GMAW, the wire works as a consumable electrode, as shown in Figure 4c below. The arc generated between the wire and the workpiece melts the wire material and deposits the molten material on the substrate's surface.

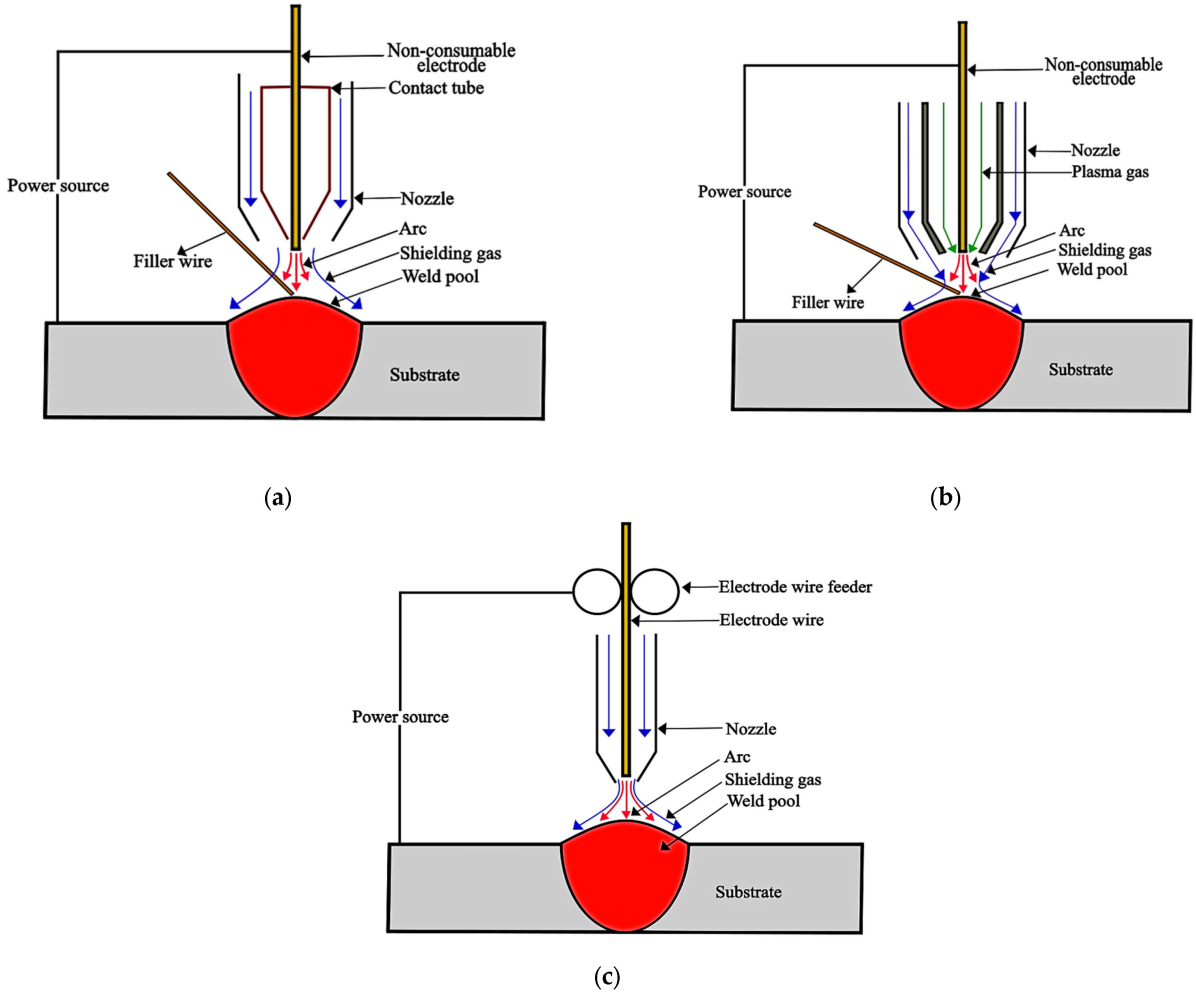

Figure 4. Types of WAAM processes. (**a**) GTAW; (**b**) PAW; (**c**) GMAW.

GMAW consists of metal inert gas (MIG) and metal active gas (MAG). In MIG, a non-reactive (inert) gas, i.e., helium or argon, is used. MIG is mainly used for non-ferrous metals. MAG uses carbon dioxide or a mixture of inert gases, i.e., a trimix of Ar + CO_2 + O_2, for shielding purposes. MAG is primarily used for ferrous metals. The material deposition rate of the GMAW process is higher as compared to other WAAM processes, and this comparison is presented below in Table 3.

Table 3. Comparison of the material deposition rates of different WAAM processes [3,19,20].

Type of AM Process	GTAW	PAW	GMAW
Material deposition rate (kg/h)	1–2	2–4	7.8

GMAW has four metal transfer modes: short-circuiting, globular, spray, and pulsed spray. Each metal transfer method has distinctive characteristics related to the welding current, equipment, and electrode type [21]. In the conventional GMAW welding process, during standard short-circuiting transfer (dip transfer) mode, when the welding electrode comes in contact with molten pool and immerses in it, short-circuiting occurs, and an enormous current flows through it. Thus, it results in the abrupt melting of the electrode wire, so droplet transfer happens via the surface tension of the molten metal pool. The arc re-ignites, and the hot process after the completion of the metal transfer process continues. A significant improvement in WAAM was achieved when the CMT (cold metal transfer) welding process was introduced. CMT is an improved version of GMAW and is based on the short-circuit transfer mode. The Austrian company "Fronius" developed the CMT method, a renowned method for generating meager heat input and high arc stability using an innovative wire feeding setup with a digital control system [22]. When the wire electrode tip comes in contact with the molten metal pool, the "robacter drive" servomotor reverses the filler wire via digital process control. Hence, it results in causing the wire to withdraw, producing droplet cutting, while the welding current quickly decreases to a near-zero value [23]. Thus, it causes lower heat input and less spatter during the material deposition. CMT can be divided into four types, i.e., CMT-conventional, CMT-advanced, CMT-pulse, and CMT-advanced pulse. Each mode has its unique features and characteristics.

2.2. General Steps Involved in WAAM Process

The main steps involved in WAAM process, as reported by literature [2,24], are presented below in Figure 5.

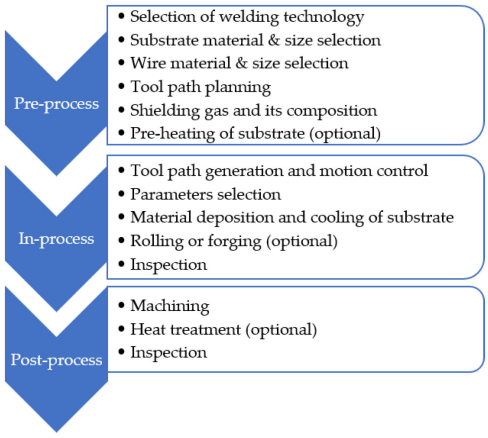

Figure 5. Steps involved in WAAM process.

2.3. Process Parameters Used in WAAM Process

2.3.1. Introduction to Different WAAM Process Parameters

The process parameters used in WAAM process vary according to the type of WAAM process and the wire material. In WAAM process, material deposition is based on melting a wire using an arc as a heat source for fabricating or repairing a component. During material deposition, the inter-pass temperature between layers increases due to the heat accumulation as further layers are added. The process parameters are crucial for producing a good-quality part, i.e., a defect-free structure with excellent mechanical properties. These process parameters include welding current, voltage, torch travel speed, wire feed speed, interlayer temperature, interlayer dwell time, shielding gas composition and flow rate, torch and substrate angle, electrode diameter, heat input, and contact tip-to-work distance (CTWD). These parameters affect the properties of WAAM product differently, and a suitable combination of these parameters is needed for specific objectives, i.e., high mechanical strength, lower surface roughness, etc.

Wire Feed Speed

Yildiz et al. [25] studied the effect of the WFS (wire feed speed) to TS (torch speed) ratio on the weld bead geometry and mechanical properties. This study showed that the WFS/TS ratio is the most crucial parameter in WAAM process for controlling heat input. Heat input is linearly correlated with the characteristic weld bead geometry, including the weld bead height, width, penetration, penetration area, and reinforcement area, for the analyzed parameter range. An inverse relationship was observed between heat input and hardness in single weld beads. Wang et al. [26] studied the effect of wire feed speed and other parameters on the weld bead geometry. This study showed that as the wire feed speed increases in GTAW-based WAAM of 4043 Al-alloy, the weld bead height increases while its width decreases. It was also reported that the arc energy required to melt the wire increases as the wire feed speed increases. Thus, it may lead to a lack of fusion and a decrease in the width of the bead. Different features of a typical weld bead are presented below in Figure 6.

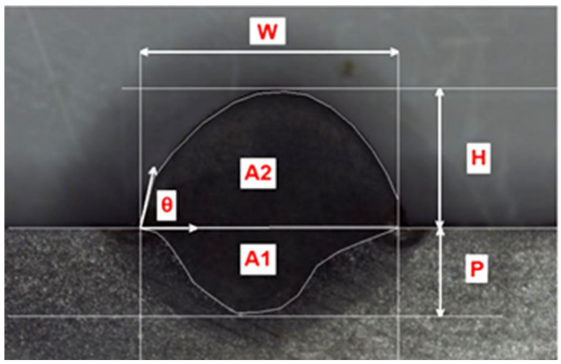

Figure 6. Schematic diagram of different weld bead features (material: ER120S-G), copyright Springer Nature, reproduced with permission [25]. where: W = Width; P = Penetration; H = Height; A1 = Penetration area; A2 = Reinforcement area; Θ = Angle of contact.

Torch Travel Speed

Dinovitzer et al. [27] examined the effect of torch travel speed and other parameters on microstructure and bead geometry in WAAM of Hastelloy X alloy. In this study, statistical tools, i.e., Taguchi and ANOVA (analysis of variance), were used to determine the effect of process parameters (wire feed, travel speed, current, and argon flow rate) on the bead's microstructure and geometry (bead shape and size, roughness, melt through depth, and oxidation level). This research revealed that current and travel speed significantly affect the weld bead's microstructure and geometry. It was revealed that torch travel speed is inversely related to the heat input in WAAM process. In WAAM process, WAAM component's microstructure depends on the heat input; hence, the part's microstructure also relies on the torch's travel speed. Furthermore, the effect of torch travel speed on the width of the weld bead was significant compared to its impact on the bead height because the travel speed affects the angle of contact (wetting angle).

Heat Input

Heat input is very critical in WAAM process. Multiple fusion and solidification cycles produce irregular heat propagation in the as-manufactured part. This non-uniform heat input accumulation and distribution defines the part's formation (shape and volume of the bead), mechanical properties, and microstructure obtained via WAAM process [28,29]. Heat input in WAAM process affects internal defect formation, phase transformation, residual stresses, and distortion [30]. Heat input can be calculated as follows from Equation (1) [31]:

$$HI = \frac{\eta UI}{TS} \quad (1)$$

where:
HI = Heat input per unit length η = Efficiency U = Voltage
TS = Travel speed I = Current

Heat input control is vital for alloys subjected to liquation cracking. As with increasing heat input, the quantity of liquated material increases, hence the chances of cracking. As WAAM process involves partial melting of the previous layer/bead, improper control of heat input will assist in partial liquation at the fusion zone [32].

Moreover, an increase in heat input will affect the cooling rates of WAAM components and, hence, the part's microstructure. As microstructure affects the part's mechanical properties, heat input indirectly affects the mechanical properties of WAAM component. Sometimes, residual stresses also arise in the part produced through WAAM process due to high heat input; in fact, that part experiences thermal stress with the deposition of each weld bead. Thus, appropriate welding technology, interlayer dwell time, and path strategy are needed to mitigate this effect.

Substrate Temperature

The substrate's pre-heat temperature defines the shape of the deposited material. As the pre-heat temperature increases, the deposited bead's width increases, whereas its height decreases [32,33]. Thus, pre-heating the substrate leads to smooth material deposition and, in return, also improves the surface deformation of the metal deposited.

Interlayer Temperature

The inter-layer temperature is crucial for obtaining the desired shape of the end product in the multi-layer WAAM process. Proper inter-layer temperature is essential for obtaining a smooth and stable surface while depositing material. Hence, properly controlling the workpiece temperature will improve its surface finish, reduce residual stress, and improve its mechanical properties [34,35]. Therefore, adequate interlayer cooling time (dwell time) is needed to get the desired interlayer temperature. This time should be chosen based on the trade-off between desired product features and production time. The idle waiting time will increase for lower inter-layer temperatures, resulting in a loss of useful production time [36].

Electrode Extension or Electrode Stick-Out

Electrode extension, or electrode stick-out, is the distance between the end part of the contact tip and the wire end, as shown in Figure 7 below. Electrical resistance increases with an increase in electrode extension. Thus, it influences the melting of the wire, and in return, it affects the weld bead geometry.

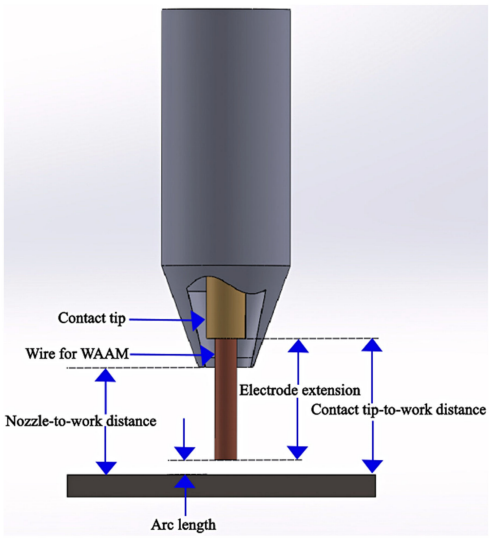

Figure 7. Electrode to work distance, arc length, and other features in MIG.

Extended electrode extension causes the pre-heating of the electrode wire. If the electrode extension is insufficient, the electrode will not get sufficiently pre-heated. Increasing the electrode extension while keeping the arc length constant enlarges the electrical resistance. More material has to be deposited due to an increment in the electrode extension but with low heat energy provided by the arc produced due to a rise in electrical resistance. In return, it will result in slight penetration and steep-crowned weld bead geometry.

Arc Length

The arc length is the distance between the welding wire tip and the substrate, as shown in Figure 7 above. The roughness of the deposited layer can be reduced by efficient control of the arc length [33].

2.4. Challenges in WAAM Process and Parameters Affecting the Product Quality

2.4.1. Defects in WAAM Process

Common defects in WAAM process include residual stresses and distortion, cracks, porosity, and humping. The process parameters that can cause such defects include wire feed speed to torch speed ratio, heat input, contact tip-to-work distance, and gas flow rate. Since in GMAW-based WAAM, the electric current is acting directly on the feedstock [37], it has more chances of problems, i.e., spattering, porosity, and excessive heating, than in GTAW-based and PAW-based WAAM.

Distortion and Residual Stresses

WAAM technology is still in the development phase, i.e., technological and process improvement. Residual stresses sometimes arise in parts produced via WAAM process due to high heat input, as shown in Figure 8. Since the component is generated via layer-by-layer deposition, WAAM generated component experiences alternating heating and cooling cycles, resulting in residual stresses and strain. If the residual stresses are high enough, they significantly affect the mechanical properties of the part produced via WAAM process. It distorts the part if the residual stresses are lower than the ultimate tensile strength (UTS) but higher than the part's yield strength (YS). If it exceeds the UTS of the part, then cracks occur in the part [38]. This problem can be resolved by selecting appropriate process parameters.

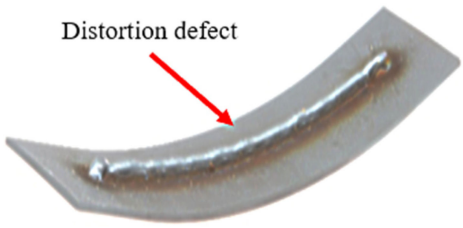

Figure 8. Distortion in part produced via WAAM process (material: ER70S-6) [39].

Porosity

One of the most common defects in WAAM aluminium alloys is porosity, as shown in Figure 9. This defect reduces the density of the part produced, and as a result, it affects the mechanical strength of the part. This defect occurs mainly due to the moisture, grease, etc., on the wire surface [31,40] or substrate. It may also arise from the entrapment of shielding or other gases in the surrounding environment. Thus, to avoid such problems, clean and smooth wire, appropriate shielding gas, a suitable mixture of gases, and a suitable flow rate of shielding gas should be used [41,42]. Interlayer cold working can also reduce this defect in the case of aluminium alloys [43]. This defect can also be reduced by increasing the cooling time of the melt pool as much as possible so that the entrapped gases get enough time to escape [44].

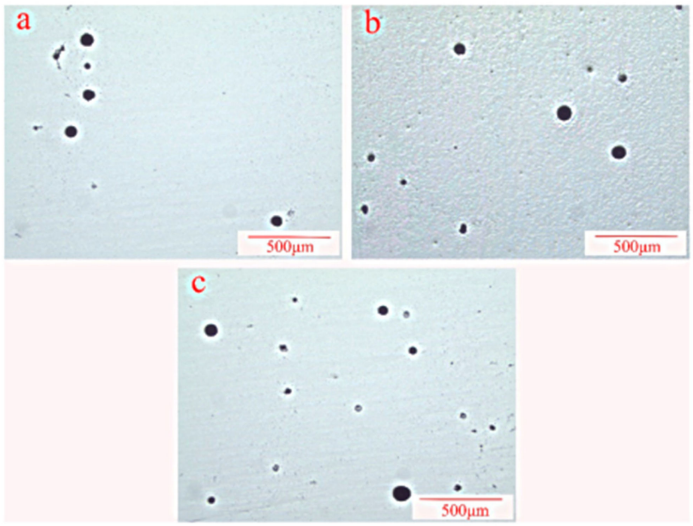

Figure 9. Pores distribution analysis with light microscopy in WAAM components produced by using three different arc modes (material: aluminium alloy 5183). (**a**) CMT + A, (**b**) CMT, and (**c**) CMT + P [45].

Humping Defect

Humping is a common defect in WAAM process, mainly due to inappropriate WFS/TS ratio use. It affects further material deposition in the process. This defect appears in the form of humps and valleys, as presented below in Figure 10. It can also be defined as the sequence of repeated undulations of the weld bead [46]. This problem can be resolved by using an appropriate WFS/TS ratio [47]. Gratzke et al. [48] used Rayleigh's instability theory and presented a theoretical concept for avoiding humping defects. In this study, the width-to-length ratio of the molten weld pool was the dominant quantity for controlling humping defects. In order to avoid humping, the width-to-length ratio of the molten weld pool has to be above a certain critical value.

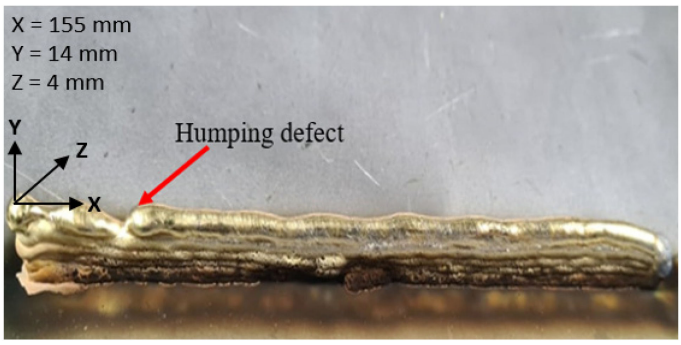

Figure 10. Humping defect (material: copper alloy CuAl8).

Material Overflow

Material overflow occurs in WAAM products, sometimes due to excessive heat accumulation. This defect occurs as a consequence of the high wettability of the molten weld pool when the interlayer dwell time (5 s) is too short, as shown in Figure 11a below. It may result in collapse, enhancing the machining allowance [49]. This problem can be avoided by using an appropriate interlayer dwell time (120 s). Thus, the next layer should be deposited when the previous layer reaches the proper temperature, i.e., by utilizing the reasonable dwell time, as shown in Figure 11b.

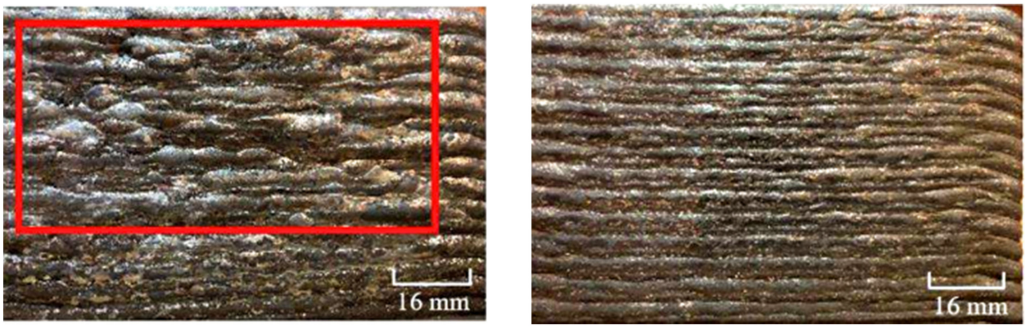

(a) (b)

Figure 11. Surface structure of walls produced by using different interpass times and keeping the torch speed constant at 10 mm/s (material: ER316LSi) [49]. (**a**) Interpass time 5 s; (**b**) Interpass time 120 s.

2.4.2. Inhomogeneous Microstructure

WAAM products usually experience complex thermal cycles. The part's microstructure, produced via WAAM process, undergoes significant changes due to different heating and cooling rates. The heat input during WAAM process significantly influences nucleation, thermal gradient, and grain growth rate [50]. This complex thermal history during material deposition results in a blended microstructure, i.e., coarse and fine. Thus, the process parameters directly impact the microstructure and strength due to multiple welding layers and related temperature cycles. Therefore, it is desirable to have a fine microstructure since it contributes to the strength of WAAM part/component. Different in-process and post-process operations for removing anisotropy in the part's microstructure are conducted depending on the applications. Different microstructures were obtained in WAAM of Ti6Al4V using different processing conditions, as shown below in Figure 12. It can be seen that the grain size and microstructure are not notably different at low interpass temperatures in regions b and c, which could be possible due to similar heat dissipation behavior. However, the microstructure becomes more uniform in region c, and the grain size increases at higher interpass temperatures due to slow cooling rates. Furthermore, when CO_2 cooling was used, a more uniform microstructure was obtained due to high cooling rates in regions b and c. The microstructure consists of an acicular α phase along with refined grains.

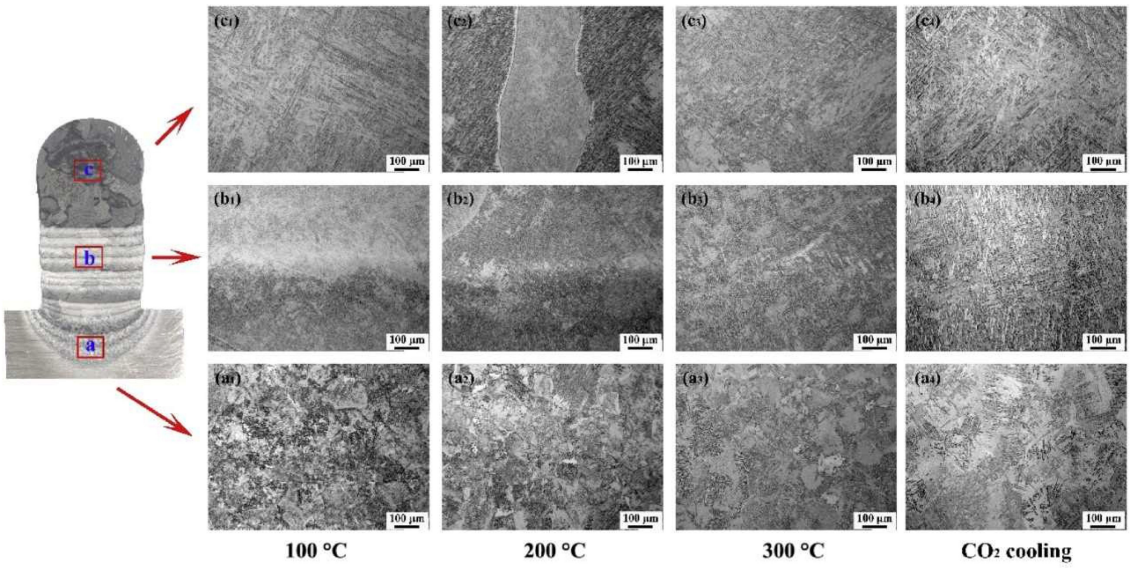

Figure 12. Variation of component's microstructure produced in WAAM process using different conditions (material: Ti6Al4V), copyright Elsevier, reproduced with permission [51].

2.4.3. Controlling Mechanical Properties of WAAM Products

The mechanical properties of the WAAM generated component depend on the microstructure, which is reliant on the heat input. Thus, controlling the part's microstructure via heat input control is a critical challenge. Furthermore, the heat input in the process will vary when different metal arc modes are used while keeping the wire feed constant [52]. Stinson et al. [53] compared the weld bead properties and geometries obtained via two different GMAW-based processes, i.e., MIG and CMT. A mild steel welding wire, ER70S-6, was used for depositing metal on EN3B substrates. This study showed that heat input significantly affects the hardness of the deposited material, as shown below in Figure 13. A decrease in heat input may be favorable for the mechanical properties and microstructure of WAAM component; however, a trade-off between heat input and production time is crucial [30]. Heat input should be selected to produce WAAM components with the desired microstructure without affecting the production time.

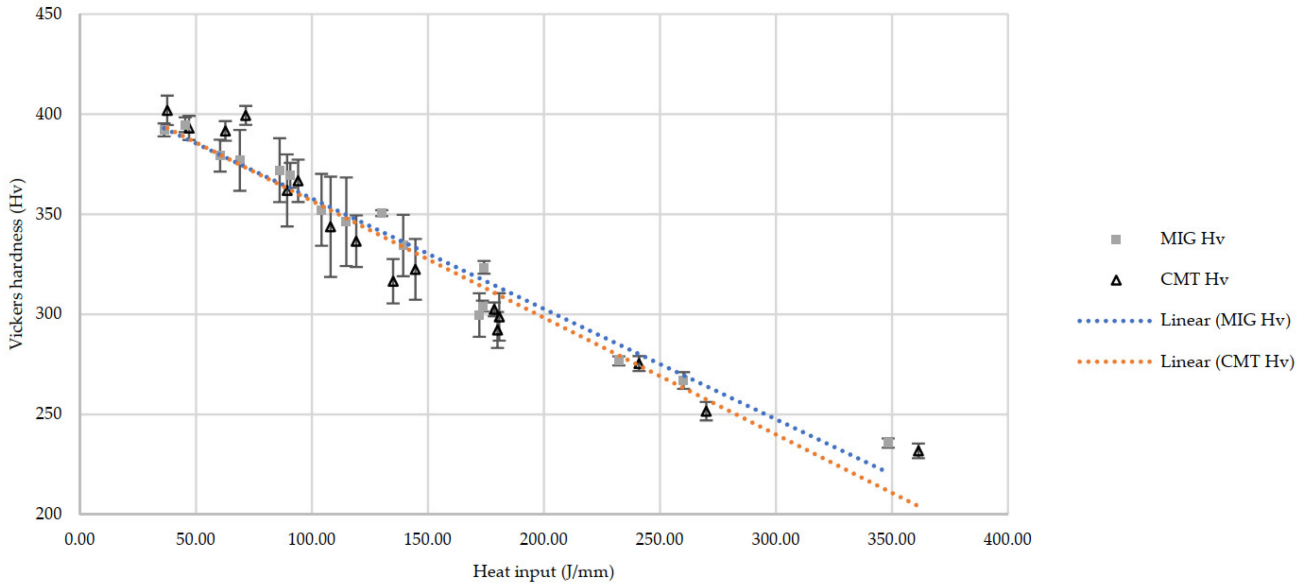

Figure 13. Hardness vs. heat input (material: ER70S-6) [53].

2.5. Methodologies to Enhance the Quality of WAAM Products

2.5.1. Optimal Process Parameters

Kumar & Anandakrishnan [54] used the Taguchi method to investigate the effect of process parameters' on the layer geometry of Inconel 825 deposited via MIG welding. Process input parameters, i.e., wire feed, welding speed, and voltage, were selected to analyze their effect on the weld bead´s width and to find the best parameters for obtaining the desired results. After statistical analysis, confirmation tests were conducted for the bead´s width using the parameter combinations found via statistical analysis. The error in the predicted values and experimental results was around 5%. Sarathchandra et al. [55] evaluated the process parameter's effect on bead characteristics in WAAM of SS304. This study used ANOVA and RSM (response surface methodology) for parameter estimation. Multiple regression models were generated for relating bead quality with process parameters and showed that the optimum process parameters for the desired bead quality are; current = 116.33 A, weld speed = 0.46 m/min, and standoff distance = 5.11 mm. Critical process parameters, their impact on quality features, and their required level in the GMAW-based WAAM process are presented below in Table 4.

Table 4. Critical process parameters for specific quality characteristics in GMAW-AM, copyright Elsevier, reproduced with permission [31].

S.No.	Quality Characteristics	Parameters Affecting the Response Characteristics	Operational Requirements
1	Bead geometry (bead width & height)	Interlayer dwell time	High
		Torch speed	High
		Welding voltage (U)	Medium
		Heat input	Medium
		Shielding gas flow rate	Medium
		Standoff distance	Medium
		Welding current (I)	Low
		Interlayer temperature	Low
		Wire feed speed	Low
		Shielding gas type	Inert (typically Ar, Ar + He)
2	Material deposition rate	Welding current (I)	High
		Electrode diameter	High
		Wire feed speed	High
		Heat input	High
		Welding voltage (U)	Medium
		Shielding gas flow rate	Medium
		Shielding gas type	Active (typically CO_2 + Ar)
3	Surface quality & porosity in the weld	Interlayer dwell time	High
		Shielding gas flow rate	High
		Welding voltage (U)	Medium
		Standoff distance	Medium
		Welding current	Low
		Heat input	Low
		Shielding gas type	Inert (Ar, Ar + CO_2, Ar + He)
4	Microstructure refinement & formation of distinct phases	Torch speed	High
		Wire feed speed	Medium
		Welding current	Medium
		Interlayer dwell time	Medium
		Shielding gas flow rate	Medium
		Welding voltage	Low
		Interlayer temperature	Low
		Heat input	Low
5	Mechanical properties (micro hardness, UTS, YS, & elongation)	Interlayer dwell time	High
		Welding current	Medium
		Heat input	Medium
		Shielding gas flow rate	Medium
		Wire feed speed	Medium
		Torch speed	Medium
		Welding voltage	Low
6	Material overflow	Interlayer dwell time	High
		Interlayer temperature	High
		Shielding gas flow rate	High
		Torch speed	High
		Heat input	Medium
		Welding current	Low
		Shielding gas type	Inert (He)
7	Spatter	Standoff distance	Medium
		Shielding gas flow rate	Medium
		Electrode diameter	Medium
		Welding voltage	Medium
		Interlayer temperature	Low
		Wire feed speed	Low
8	Corrosion resistance	Interlayer dwell time	High
		Torch speed	High
		Shielding gas flow rate	Medium
		Welding current	Low
		Wire feed speed	Low
		Heat input	Low
		Shielding gas type	Inert (typically Ar, He, Ar + He)

2.5.2. Path Strategy

Single Bead Multiple Passes

Lehmann et al. [56] studied two tool paths for material deposition, i.e., unidirectional and bidirectional material deposition strategies, as shown in Figure 14a,b, respectively. The welding torch nozzle traverses these two paths while fabricating a single-track wall, where the electric arc is turned on or off. The two material deposition strategies differ in that the material is deposited only from the start to the end position in the unidirectional material deposition strategy. In contrast, during the bi-directional material deposition strategy, the material layer was deposited when the torch moved in each direction.

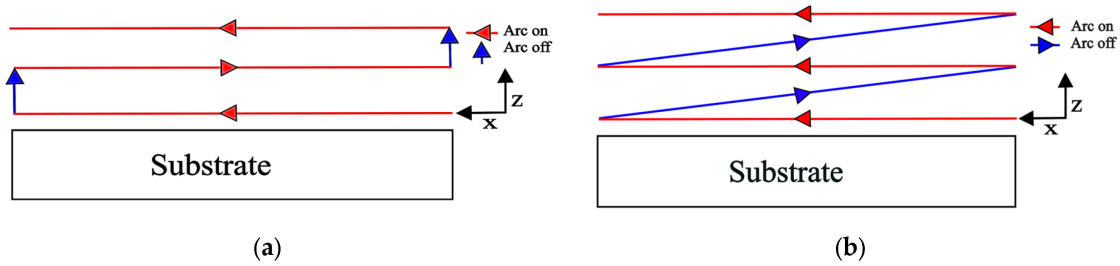

Figure 14. Path strategy. (**a**) Unidirectional material deposition; (**b**) Bidirectional material deposition.

This research showed that when fabricating a single-track wall using a unidirectional material deposition strategy, the material accumulated on the starting side and formed a bulging area on the starting side of the wall. At the same time, it caused a reduction in material deposition at the end of the wall. This problem can be overcome by controlling the WFS and TS [56]. However, it was resolved easily via a bidirectional material deposition strategy, shown in Figure 14b, because the extra initial material flow was balanced on both ends.

Multiple Beads, Multiple Passes

Suryakumar et al. [19] developed a second-degree regression model based on the experimental data obtained. Bead geometry was defined as a function of the TS and WFS. It was assumed that the bead's geometry is similar to a parabola, and this supposition was extended to a multi-bead material deposition model. Since additional material was not considered in the overlapping zone between two adjacent beads, the results were not reliable and accurate. The suggested model was then improved by introducing a fillet between two consecutive weld beads, as shown in Figure 15 below.

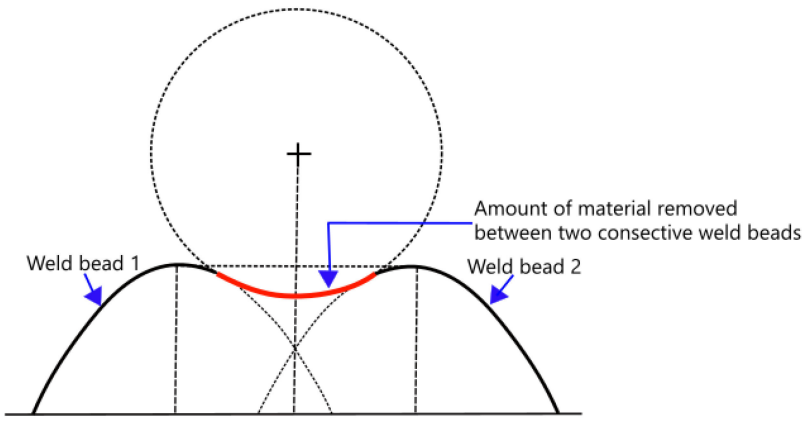

Figure 15. Overlapping parabolic bead model with fillet between two consecutive beads, according to [19].

Later, Ding et al. [57] used parabola, cosine, and arc functions to study and present an accurate single-bead model. The experimental data-based curve fitting showed that

the parabola and cosine models could represent the single weld bead optimally. This research study further suggested that the tangent overlapping model (TOM) can be used for higher accuracy and efficient material deposition in the multi-bead WAAM process compared to the traditional flat-top overlapping model (FOM). The TOM model is based on the idea of critical valley areas and overlapping areas. The TOM model presented that for multi-bead deposition, the optimal center distance (d_{opt}) between two beads is $d_{opt} = 0.738w$ (w = width of weld bead), as shown in Figure 16. The material yield (volume of part remaining/volume deposited) was 84.1%, using $d_{opt} = 0.738w$.

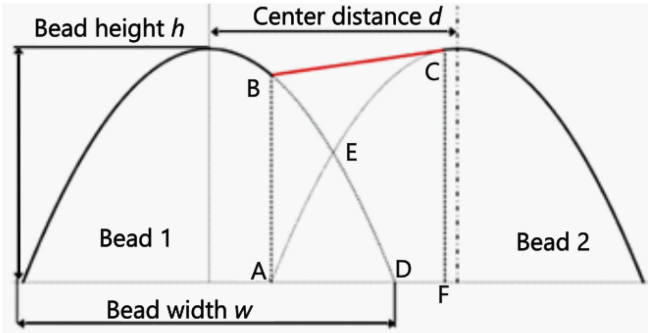

Figure 16. Multi bead deposition model, copyright Elsevier, reproduced with permission [57].

2.5.3. Appropriate Shielding Gas

In WAAM process, shielding gas type and flow rate can affect the product's quality. The leading role of the shielding gas is to protect the molten metal pool from reacting with atmospheric gases and prevent the quality of the weld bead from degradation. In addition, it affects the overall quality of the weld bead, i.e., arc stability, preventing surface oxidation, porosity, and slag formation [58,59]. Each gas or gas mixture has unique characteristics that may affect the overall quality of the weld bead and its mechanical properties. Therefore, special attention should be given to shielding gas selection before starting a WAAM process.

The shielding gas selection depends on the material of the wire used in WAAM process and the quality requirements of WAAM component [31]. In some cases, inert gas is used alone for shielding purposes, but sometimes different types of gases are mixed in a fixed proportion to obtain a good-quality weld bead with less spatter. A summary of the different shielding gases used by various researchers in WAAM process is presented below in Table 5.

Table 5. Shielding gases used in WAAM with particular electrode material.

Metal Alloys	Alloy Grade (Filler Wire)	Shielding Gas	References
Aluminium alloys	ER2319	99.99% Ar	[60,61]
	ER4043 (Al5Si)	99.99% Ar	[62–64]
	Al-4047	99.99% Ar	[65]
	ER4220	99.99% Ar	[66]
	ER5083	99.99% Ar	[60]
	ER5153	99.99% Ar	[67]
	ER5183 (AA5183)	99.99% Ar	[68]
	ER5356	99.99% Ar	[69–71]
		95% Ar + 5% CO_2	[72]
	5A06	99.99% Ar	[73]
	Al-6Mg	99.99% Ar	[74]
	AlCu4.3 Mg1.5	99.99% Ar	[75]
Steel alloys	304 Stainless steel	99.99% Ar	[76]
	304L	99.99% Ar	[77]
		99.99% Ar	[78,79]
	308L (YS308L)	90% He + 7.5% Ar + 2.5% CO_2	[80]
		98% Ar + 2% CO_2	[81]

Table 5. *Cont.*

Metal Alloys	Alloy Grade (Filler Wire)	Shielding Gas	References
	ER308LSI	98% Ar + 2% CO_2	[82]
		90% He + 7.5% Ar + 2.5% CO_2	[83]
	316L	98% Ar + 2% CO_2	[37,84]
		97.5% Ar + 2.5% CO_2	[85]
		99.99% Ar	[86,87]
	ER316LSi	90% Ar + 10% CO_2	[88]
	ER110S-G	82% Ar + 18% CO_2	[89]
		99.99% Ar	[90]
	ER120S-G	80% Ar + 20% CO_2	[25]
		99.99% Ar	[91,92]
	ER70S-6 (Mild steel)	80% Ar + 20% CO_2	[93–97]
		82% Ar + 18% CO_2	[89]
		90% Ar + 10% CO_2	[88]
		95% Ar + 5% CO_2	[91,92]
		98% Ar + 2% CO_2	[84]
		75% Ar + 25% CO_2	[83]
		Dry air at 0.6 MPa	[98]
	G3Si1 (Mild steel)	82% Ar + 18% CO_2	[99]
		99.99% Ar	[100]
	H08Mn2Si	95% Ar + 5% CO_2	[101–114]
	ER90S-B91 (P91)	99.99% Ar	[115]
	2Cr13	97.5% Ar + 2.5% CO_2	[116,117]
	ER2594	99.99% Ar	[118]
	H13 tool steel	99.99% Ar	[119,120]
	Bainite steel	95% Ar + 5% CO_2	[121]
Nickel alloys	Monel K500	99.99% Ar	[122]
	ERNiCu-7 (FM60)	99.99% Ar	[122]
	Inconel 625	99.99% Ar	[123,124]
		97.5% Ar + 2.5% CO_2	[124]
		95.5% Ar + 3% He + 1.5% H_2	[124]
		95% Ar + 5% H_2	[124]
		70% Ar + 30% He	[125]
	IN625B	99.99% Ar	[126]
	Ni6082	99.99% Ar	[78,81]
	Inconel 718	99.99% Ar	[127]
Titanium alloys	Ti-6Al-4V (Ti-64)	99.99% Ar	[128–131]
	Ti-6.5Al-3.5Mo-1.5Zr-0.3Si	99.99% Ar	[132]
	Ti-3Al-8V-6Cr-4Mo-4Zr (Beta-C)	99.99% Ar	[133]
Magnesium (Mg) alloys	AZ80M	99.99% Ar	[134]
	AZ31	99.99% Ar	[135]
	AZ91	99.99% Ar	[136]
Copper & its alloys	Cu wire (99.99% pure)	99.99% Ar	[137]
	CuSi3Mn1	99.99% Ar	[138]
	Cu-8Al-2Ni-2Fe-2Mn	99.99% Ar	[139]
	ERCuAl-A2	99.99% Ar	[140]
	CuSi3	99.99% Ar	[141,142]
	CuAl8	99.99% Ar	[143]
Cobalt alloys	Stellite-6	70% Ar + 30% He	[144]

2.5.4. In-Process Operations in WAAM Process for Quality Improvement

Hybrid WAAM Process

Hybrid WAAM uses additional machining and WAAM processes to get the desired geometry. It reduces the chances of material overflow and reduces the excessive machining at the end of the WAAM process. Hybrid WAAM can also improve mechanical properties, i.e., through grain refining. Furthermore, it can also be used to reduce defects in WAAM-

generated components. A detailed overview of hybrid WAAM processes is shown below in Table 6.

Table 6. Types of hybrid WAAM processes.

Operation	Wire Type	Welding Type	Effects of Hybrid WAAM	References
In-process milling	Aluminium alloy ER4043	CMT (Pulse)	(a) For milling thickness (t) 0.4–1.2 mm, surface roughness, and machining allowance were reduced by 22.9% and 31.6%, respectively (b) When t is increased to 1.6 mm, the surface texture becomes rough and poor	[145]
Interlayer hot forging	AISI316L	MIG	(a) Improvement in yield and ultimate tensile strength (b) Elongation to fracture and the number of pores is reduced	[146]
In-process rolling	ER70S-6	CMT	(a) Reduction in residual stresses and distortion and slotted roller was more effective (b) Improvement in grain refinement	[93]

Depending on the application, different profile rollers can be used for in-process rolling in WAAM process. A typical hybrid WAAM process is shown in Figure 17 below. The significant advantage of the rolling process is that plastic deformation over the entire weld cross-section can be induced instead of only at the surface. It diminishes the residual stress induced during welding more adequately [93].

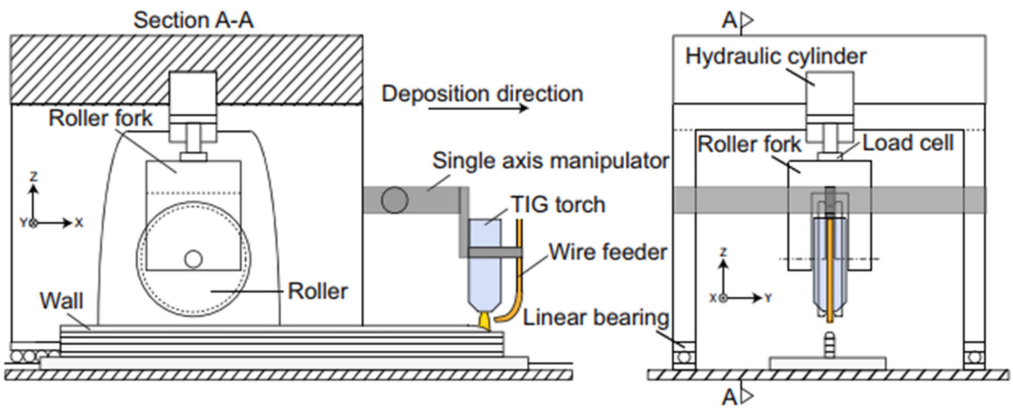

Figure 17. Hybrid WAAM process (WAAM + Rolling), copyright Elsevier, reproduced with permission [93].

Additional Steps for Improving Material Properties

In WAAM process, additional in-process operations are utilized to meet the product quality requirements and obtain the desired features. It includes restraining material overflow, lower surface roughness, less waviness, and a homogeneous part´s microstructure. A brief overview of the different in-process operations used in WAAM is presented below in Table 7.

2.5.5. Post-Process Operations

Milling (Mandatory)

The assembled part must be entirely reworked by milling operations to ensure quality and accuracy requirements. For this purpose, the well-known technology of CNC milling with multi-axial machining is used. The parameters and tools for milling are selected

depending on the material properties of WAAM product. For this purpose, the cutting values known from the conventional areas are adapted. A typical part with and without post-process milling is shown below in Figure 18.

Table 7. In-process operations in WAAM process for improving material properties.

Operation		Wire Type	Welding Type	Effect of In-Process Operation	References
Interlayer cooling	Thermoelectric cooling	Aluminium alloy 2325	Tandem-GMAW	(a) Better control of molten pool shape (b) Reduction in the interlayer delay time	[147]
	Air jet cooling	ER70S-6	MIG	(a) Increase in the height of the deposited material wall between 0.5–2.0 mm (b) Decrease in deposition efficiency by up to 10%	[148]
Ultrasonic peening		Ti-6Al-4V	CMT	(a) Improvement in tensile strength and anisotropy in tensile strength was reduced to 0.8% from 6%	[128]
In-process wire heating		Ti-6.5Al-3.5Mo-1.5Zr-0.3Si	GTAW	(a) With an increase in the wire heating, the differences in tensile strength and elongation rate in the scanning and deposition direction disappeared by obtaining equiaxed grains	[132]

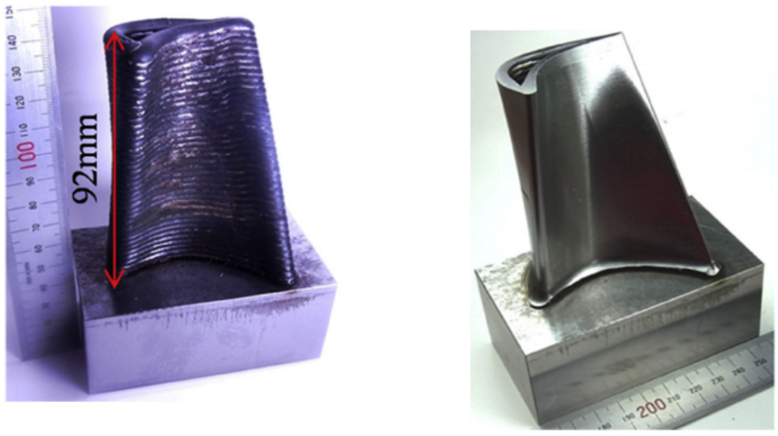

(**a**) (**b**)

Figure 18. Post-process milling of WAAM product (material: SS400). (**a**) Before milling (Ra 0.2 mm); (**b**) After milling (Ra 0.8 µm) [149].

Other Non-Mandatory Post-Process Operations (Optional)

Different post-process operations are utilized over time to improve the quality of WAAM generated components. Heat treatment is one of the post-process operations that is sometimes used to improve the mechanical strength of the part and reduce the residual stresses induced during the WAAM process. Post-process heat treatment improves grain refinement, especially in the case of Inconel and aluminium alloy [150]. Generally, materials with high carbon contents are recommended for post-process heat treatment [43]. Selection of the heat treatment process is crucial as it may increase the chances of cracking

in some materials during mechanical loading due to existing thermal stresses in part using inaccurate heat treatment. Thus, post-process heat treatment should be selected according to the type of material and application of WAAM component [150].

2.5.6. Process Monitoring

Although WAAM is an exemplary process for producing large parts and components, the process's control and stability are crucial due to the arc-based material deposition process and long cycle time. Real-time monitoring of the material deposition process and feedback on the deposition state are vital. Defects produced in WAAM process are usually associated with different types of signal generation, i.e., acoustic, optical, thermal, etc. The quality of WAAM products can be ensured by accurately sensing these signals. A detailed overview of different methods used for monitoring various features of WAAM process is presented below in Table 8.

Table 8. Monitoring methods in WAAM process.

Monitoring Method	Feature Monitored	References
Acoustic based monitoring	Arc length	[151]
	CTWD	[152]
	Metal transfer modes	[153]
	Material deposition efficiency	[154]
Optical based monitoring	Deviations in wire-feeding position	[155]
	Layer height	[156,157]
	Bead geometry	[112,158–160]
	Arc length	[161–163]
	Defect detection (porosity)	[44]
	Melt pool size	[164]
Thermal based monitoring	Interlayer temperatures	[165,166]
	Geometry of melt pool	[167]
	Strain fields evaluation	[168]
	Defects detection	[169]
Spectroscopy based monitoring	Defects detection	[170,171]
	Layer Width	[172]
Electrical based monitoring	Forming quality	[63]
	Deposition height	[173]

3. A Brief Overview of Different Wire Materials Used in WAAM Process

3.1. Single-Wire WAAM Process

In the single-wire WAAM process, only a single wire is fed into the molten metal pool for deposition. Multiple studies have been conducted for depositing different types of metals/alloys, including copper and its alloys, aluminium alloys, steel, titanium alloys, and magnesium alloys. The filler material is primarily available as a spool and controlled through a wire feeder. A detailed summary of metals/alloys and different types of energy sources used in WAAM process for depositing these metals/alloys is presented below in Table 9.

3.2. Multi-Wires WAAM Process

In the multi-material WAAM process, more than one wire is fed into the molten metal pool for deposition. Different industries are competing to achieve high functional integrity and a reduction in the weight of WAAM-based components due to their economic and environmental advantages. Hybrid materials are usually deposited to improve the features of WAAM-based components, i.e., hardness, toughness, tensile strength, and weight. It is stated in the literature [199] that one of the main challenges in the processing of hybrid materials in additive manufacturing is cracking in the transition zones of materials as a consequence of brittle phases, which are in turn caused by the blending of different

materials or by differences in thermal expansion coefficients. However, Hauser et al. [200] showed that properties in components produced through the multi-wire WAAM process using two different aluminium alloy wires are limited by individual material properties and not by the transition zone of the material. A detailed summary of multi-wires and various types of energy sources used in WAAM process is presented below in Table 10.

Table 9. Types of wire materials used in WAAM process.

Metal Alloys	Alloy Grade (Filler Wire)	Source of Energy	References
Aluminium alloys	ER2319	GTAW, CMT, CMT-PA & MIG-P	[61,174,175]
	Al-4047 & Al-5356	CMT	[65]
	5A06	GTAW	[73]
	ER-4043 (Al5Si)	CMT Advanced, MIG/MAG	[176,177]
	ER5356	GTAW	[178]
	ER4220	CMT	[66]
	AA5183	GMAW	[179]
Steel	Stainless steel	PAW	[180]
	Steel (H08Mn2Si)	MIG & TIG	[101]
	Mild steel (ER70S-6)	CMT, MIG, TIG	[93,181,182]
	SS308 L	GMAW	[183]
	ER90S-B91 (P91)	PAW	[115]
	2Cr13	CMT	[116]
	SS 316 (ER316LSi)	PAW	[184]
Nickel alloys	Inconel 718	GMAW	[184]
	Inconel 625	CMT, PAW-P	[185,186]
	IN625B	GTAW	[126]
Titanium alloys	Ti-6Al-4V (Ti-64)	PAW, GTAW, GTAW-P	[184,187–191]
	Ti-6.5Al-3.5Mo-1.5Zr-0.3Si	GTAW	[132]
	Ti-3Al-8V-6Cr-4Mo-4Zr (Beta-C)	GTAW	[133]
	Ti-64 & Ti-5Al-5V-5Mo-3Cr (Ti-5553)	GTAW	[192]
Magnesium (Mg) alloys	AZ80M	GTAW-P, GTAW	[134,193]
	AZ31	GTAW, CMT	[136,194–196]
	AZ91	GTAW	[136]
Copper and its alloys	Cu wire (99.99% pure)	GMAW	[137]
	CuSi3Mn1	CMT	[138]
	Cu-8Al-2Ni-2Fe-2Mn	-	[139,197]
	Cu-Al8Ni2Fe2	CMT, CMT-P	[198]
	CuSi3	CMT	[141,142]
	CuAl8	CMT	[143]
	ERCuAl-A2	GTAW	[140]

Table 10. Materials used in the multi-material WAAM process.

S.No.	Alloy Grade	Source of Energy	References
1	AA6060 & AA5087	CMT, CMT+P	[200]
2	SS321 (ER321) & Inconel 625 (ER625)	-	[201]
3	ER70s-6 & ER316L	CMT	[88,202]
4	ERCuAl-A2 & ER-120S-G	GTAW	[140]

3.3. WAAM of Copper-Based Materials

Copper is a highly conductive non-ferrous metal with a reddish appearance. Apart from that, copper has medium strength, good formability, and excellent corrosion resistance. Its thermal and electrical conductivity is only second to silver's. For some applications, the properties of pure copper may not be adequate. Hence, a small amount of an alloying element is added for this purpose, leading to the development of many copper alloys. Adding small alloying elements can significantly improve pure copper's properties, i.e.,

strength, machinability, and softening temperature [203]. It should be noted that the properties of the alloy depend on the metal added to it. For example, the addition of nickel results in higher corrosion resistance, and due to this property, CuNi alloys are used in marine structures. Similarly, its properties differ when aluminium is added, resulting in increased strength. However, the addition of impurities may affect the conductivity of the copper. A list of the typical copper-based filler wires and rods used for welding and their composition is presented in Table 11.

Table 11. Chemistry of copper-based filler wires and rods, according to [204–206].

AWS Class	DIN EN ISO (24373)	Common Name	Contents of Primary Elements (%)											
			Cu	Sn	Mn	Fe	Pb	Si	Ni	P	Al	Ti	Zn	Ag
ERCu	S Cu 1898	Copper	Rem	0.8	0.3	0.05	-	0.3	-	-	0.01	-	-	-
	S Cu 1897	CuAg1	Rem	-	0.06	-	-	-	-	0.01	-	-	-	1
ERCuSi-A	S Cu 6560	Silicon bronze	Rem	1	1.5	0.5	-	2.8–4	-	-	0.01	-	1	-
ERCuSn-A	S Cu 5180	Phosphor bronze	Rem	4–6	-	-	-	-	-	0.1–0.35	0.01	-	-	-
ERCuSn-C	S Cu 5210	Phosphor bronze	Rem	7–9	-	0.1	0.02	-	-	0.1–0.35	0.01	-	0.2	-
ERCuNi	S Cu 7158	Copper-nickel	Rem	-	1	0.4–0.75	-	0.25	29–32	0.02	-	0.2–0.5	-	-
ERCuAl-A1	S Cu 6100	Aluminium bronze	Rem	-	0.5	-	-	0.1	-	-	6–8.5	-	0.2	-
ERCuAl-A2	S Cu 6180	Aluminium bronze	Rem	-	-	1.5	-	0.1	-	-	8.5–11	-	0.02	-
ERCuAl-A3	S Cu 6240	Aluminium bronze	Rem	-	-	2–4.5	-	0.1	-	-	10–11.5	-	0.1	-
ERCuNiAl	S Cu 6328	Nickel aluminium bronze	Rem	-	0.6–2.5	3–5	-	0.1	4–5.5	-	8.5–9.5	-	0.1	-
ERCuMnNiAl	S Cu 6338	Manganese-nickel aluminium bronze	Rem	-	11–14	2–4	-	0.1	1.5–3	-	7–8.5	-	0.15	-

Most copper-based alloys are arc weldable, but this weldability is lower than that of steel. The main challenge with such types of materials is their high thermal conductivity. Furthermore, applications of these copper-based filler wires are given below in Table 12.

Table 12. Features and typical applications of copper-based filler metals, according to [204–206].

Common Name	AWS Class	DIN EN ISO (24373)	Feature	Typical Applications
Copper	ECu ERCu	S Cu 1898	• Good corrosion resistance • Poor electrical conductivity	• Deoxidized copper welding • Tough-pitch copper welding
Phosphor bronze	ECuSn-A ERCuSn-A ECuSn-C ERCuSn-C	S Cu 5180 S Cu 5210	• Good mechanical wear resistance	• Bearings overlay • Welding of copper, brass, and phosphor bronze
Silicon bronze	ECuSi ERCuSi-A	S Cu 6560	• Due to low thermal conductivity, it has an excellent molten metal fusion	• Welding of brass, copper, and silicon bronze • Resistance to seawater and chemicals
Nickel aluminium bronze	ECuNiAl ERCuNiAl	S Cu 6328	• Good protection against corrosion, cavitation, and erosion in saline & brackish water	• Used for welding cast or wrought Ni-Al bronzes
Copper-nickel	ECuNi ERCuNi	S Cu 7158	• Good protection against seawater • No need for pre-heating due to hot shortness	• Used for welding cast or wrought copper-nickel alloys • Its claddings are resistible to the seawater
Manganese-nickel aluminium bronze	ECuMnNiAl ERCuMnNiAl	S Cu 6338	• Excellent protection against corrosion, cavitation & erosion	• Welding of cast or wrought manganese-nickel aluminium bronzes
Aluminium bronze	ECuAl-A2 ECuAl-B ERCuAl-A1 ERCuAl-A2 ERCuAl-A3	S Cu 6100 S Cu 6180 S Cu 6240	• Good protection against chemical & saline water • Good protection against mechanical wear	• Used for welding the Cu-Al alloys (ERCuAl-A1 is only used for surfacing) • Used for repairing welds in ships, marine propellers & chemical machinery & cylinders

The high reflectivity, thermal conductivity, and surface oxide formation complicate the welding of pure copper and its alloys. During WAAM process of such materials, rapid

heat dissipation is observed, resulting in high residual stresses and distortion. A detailed overview of WAAM for copper-based materials is presented below in Table 13.

Table 13. Recent studies on WAAM of copper-based materials.

Electrode Material	Area of Study	References
CW1860 **Bare Cu wire (99.99% pure)**	1. Investigation of pure copper deposition 2. Investigation of electrical conductivity dependency on wire type and shielding gas used for depositing copper	[207]
Cu wire (99.99% pure)	1. To investigate the feasibility of depositing pure copper via WAAM process	[137]
Copper wire (99.99% pure) & 1080 aluminium wire	1. To study the feasibility of obtaining a Cu-Al alloy using two different wires 2. Investigating alloy composition, mechanical properties, and effect of heat treatment on alloy homogenization	[208]
CuSi3Mn1	1. Study of the microstructure developed during pulsed and short-circuiting metal transfer modes 2. Optimize the deposition parameters in these two modes	[138]
Cu-Al8Ni2Fe2	1. To study the feasibility of creating large components via WAAM process 2. To study mechanical and corrosion-related properties of the deposited material	[198]
Cu-8Al-2Ni-2Fe-2Mn	1. To investigate the location effect on mechanical properties and microstructure of the NAB alloy deposited structure	[139]
	1. To study the effect of interlayer temperature on mechanical properties and microstructure with and without ultrasonic vibrations	[197]
ERCuAl-A2 & ER-120S-G	1. Fabrication and investigation of functionally graded material using the T-WAAM process	[140]
CuSi3 & ER4043	1. To investigate the fabrication of Cu6.6%Al-3.2%Si alloy using twin wires and to standardize the process parameters 2. To study the mechanical properties of the deposited alloy	[141]
	1. To develop a customized alloy by feeding two different wires simultaneously into the weld pool 2. To investigate the mechanical properties of the deposited alloy by varying Si and Al contents in the weld pool by changing the wire feed	[142]
CuAl8	1. To analyze the interpass temperature during WAAM of CuAl8	[143]

4. Conclusions and Future Research Directions

WAAM-based processes have the strong potential to dominate the AM industry in the near future due to their superior features compared to other methods. These properties include a shorter lead time, low material waste, and low energy consumption. A comprehensive review of the different aspects related to WAAM process has been presented in this paper. This paper includes various challenges faced in WAAM process, including in-process and post-process operations, process monitoring, shielding gases, and materials

used in WAAM process. The major highlights of this review paper and future research directions related to WAAM process can be summarized as follows:

a. WAAM is a promising technology for fabricating parts/components with complex geometries. It has been explored for metal alloys such as steel, aluminium, etc. However, it should be explored further for new advanced materials such as functionally graded materials;
b. Material deposition in WAAM process is generally accompanied by different types of defects and challenges, i.e., material overflow, poor weld bead quality, humping defects, etc. These problems can be addressed via suitable parameter selection and an optimal material deposition strategy;
c. In-process operations, i.e., rolling, forging, etc., can enhance the microstructure and mechanical properties of simple WAAM products. However, for complex geometries, suitable in-process operations need to be developed. Furthermore, post-process operations are also crucial for enhancing microstructure and mechanical properties;
d. Defect generation is associated with different signals, i.e., optical, thermal, etc. These signals can be sensed accurately by employing an advanced signal detection system to ensure and improve the quality of WAAM products. Furthermore, non-destructive testing techniques should be utilized to assess the in-service performance and life of WAAM products;
e. It was found that the correlation between process parameters and part quality has not yet been sufficiently explored. It should be further investigated using the specific test methodology, and the relationship should be described as a model. Hence, a WAAM process that meets quality requirements can be developed in the planning phase.

Author Contributions: Conceptualization, A.S. and R.A.; methodology, R.A.; validation, R.A., H.Z., and S.K.; formal analysis, A.S. and S.K.; investigation, A.S.; resources, A.S. and S.K.; data curation, A.S. and R.A.; writing—original draft preparation, A.S., R.A. and S.K.; writing—review and editing, H.Z. and R.A.; visualization, R.A. and S.K.; supervision, A.S.; All authors have read and agreed to the published version of the manuscript.

Funding: Open Access Funding by the Publication Fund of TU Bergakademie Freiberg.

Data Availability Statement: Data are contained within the article.

Conflicts of Interest: The authors declare no conflict of interest.

References

1. Karakurt, I.; Lin, L. 3D Printing Technologies: Techniques, Materials, and Post-Processing. *Curr. Opin. Chem. Eng.* **2020**, *28*, 134–143. [CrossRef]
2. Raut, L.P.; Taiwade, R.V. Wire Arc Additive Manufacturing: A Comprehensive Review and Research Directions. *J. Mater. Eng. Perform.* **2021**, *30*, 4768–4791. [CrossRef]
3. Li, Y.; Su, C.; Zhu, J. Comprehensive Review of Wire Arc Additive Manufacturing: Hardware System, Physical Process, Monitoring, Property Characterization, Application and Future Prospects. *Results Eng.* **2021**, *13*, 100330. [CrossRef]
4. Pagac, M.; Hajnys, J.; Ma, Q.-P.; Jancar, L.; Jansa, J.; Stefek, P.; Mesicek, J. A Review of Vat Photopolymerization Technology: Materials, Applications, Challenges, and Future Trends of 3D Printing. *Polymers* **2021**, *13*, 598. [CrossRef] [PubMed]
5. Alfattni, R. Comprehensive Study on Materials Used in Different Types of Additive Manufacturing and Their Applications. *Int. J. Math. Eng. Manag. Sci.* **2022**, *7*, 92. [CrossRef]
6. Lv, X.; Ye, F.; Cheng, L.; Fan, S.; Liu, Y. Binder Jetting of Ceramics: Powders, Binders, Printing Parameters, Equipment, and Post-Treatment. *Ceram. Int.* **2019**, *45*, 12609–12624. [CrossRef]
7. Gülcan, O.; Günaydın, K.; Tamer, A. The State of the Art of Material Jetting—A Critical Review. *Polymers* **2021**, *13*, 2829. [CrossRef]
8. Gibson, I.; Rosen, D.W.; Stucker, B.; Khorasani, M.; Rosen, D.; Stucker, B.; Khorasani, M. *Additive Manufacturing Technologies*; Springer: Berlin/Heidelberg, Germany, 2021; Volume 17.
9. Thapliyal, S. Challenges Associated with the Wire Arc Additive Manufacturing (WAAM) of Aluminum Alloys. *Mater. Res. Express* **2019**, *6*, 112006. [CrossRef]
10. Lehmann, T.; Rose, D.; Ranjbar, E.; Ghasri-Khouzani, M.; Tavakoli, M.; Henein, H.; Wolfe, T.; Jawad Qureshi, A. Large-Scale Metal Additive Manufacturing: A Holistic Review of the State of the Art and Challenges. *Int. Mater. Rev.* **2022**, *67*, 410–459. [CrossRef]

11. Svetlizky, D.; Das, M.; Zheng, B.; Vyatskikh, A.L.; Bose, S.; Bandyopadhyay, A.; Schoenung, J.M.; Lavernia, E.J.; Eliaz, N. Directed Energy Deposition (DED) Additive Manufacturing: Physical Characteristics, Defects, Challenges and Applications. *Mater. Today* **2021**, *49*, 271–295. [CrossRef]
12. Frazier, W.E. Metal Additive Manufacturing: A Review. *J. Mater. Eng. Perform.* **2014**, *23*, 1917–1928. [CrossRef]
13. Zhai, W.; Wu, N.; Zhou, W. Effect of Interpass Temperature on Wire Arc Additive Manufacturing Using High-Strength Metal-Cored Wire. *Metals* **2022**, *12*, 212. [CrossRef]
14. Rodrigues, T.A.; Duarte, V.; Miranda, R.M.; Santos, T.G.; Oliveira, J.P. Current Status and Perspectives on Wire and Arc Additive Manufacturing (WAAM). *Materials* **2019**, *12*, 1121. [CrossRef] [PubMed]
15. Zhang, Y.M.; Li, P.; Chen, Y.; Male, A.T. Automated System for Welding-Based Rapid Prototyping. *Mechatronics* **2002**, *12*, 37–53. [CrossRef]
16. Zhang, Y.; Chen, Y.; Li, P.; Male, A.T. Weld Deposition-Based Rapid Prototyping: A Preliminary Study. *J. Mater. Process. Technol.* **2003**, *135*, 347–357. [CrossRef]
17. Xiong, J.; Zhang, G. Adaptive Control of Deposited Height in GMAW-Based Layer Additive Manufacturing. *J. Mater. Process. Technol.* **2014**, *214*, 962–968. [CrossRef]
18. Ahn, D.-G. Direct Metal Additive Manufacturing Processes and Their Sustainable Applications for Green Technology: A Review. *Int. J. Precis. Eng. Manuf.-Green Technol.* **2016**, *3*, 381–395. [CrossRef]
19. Suryakumar, S.; Karunakaran, K.P.; Bernard, A.; Chandrasekhar, U.; Raghavender, N.; Sharma, D. Weld Bead Modeling and Process Optimization in Hybrid Layered Manufacturing. *Comput.-Aided Des.* **2011**, *43*, 331–344. [CrossRef]
20. Liu, J.; Xu, Y.; Ge, Y.; Hou, Z.; Chen, S. Wire and Arc Additive Manufacturing of Metal Components: A Review of Recent Research Developments. *Int. J. Adv. Manuf. Technol.* **2020**, *111*, 149–198. [CrossRef]
21. Tawfik, M.M.; Nemat-Alla, M.M.; Dewidar, M.M. Enhancing the Properties of Aluminum Alloys Fabricated Using Wire+ Arc Additive Manufacturing Technique—A Review. *J. Mater. Res. Technol.* **2021**, *13*, 754–768. [CrossRef]
22. Tian, C.L.; Chen, J.L.; Dong, P.; He, J.W.; Wang, Y.J. Current State and Future Development of the Wire Arc Additive Manufacture Technology Abroad. *Aerosp. Manuf. Technol.* **2015**, *2*, 57–60.
23. Furukawa, K. New CMT Arc Welding Process–Welding of Steel to Aluminium Dissimilar Metals and Welding of Super-Thin Aluminium Sheets. *Weld. Int.* **2006**, *20*, 440–445. [CrossRef]
24. Taşdemir, A.; Nohut, S. An Overview of Wire Arc Additive Manufacturing (WAAM) in Shipbuilding Industry. *Ships Offshore Struct.* **2021**, *16*, 797–814. [CrossRef]
25. Yildiz, A.S.; Davut, K.; Koc, B.; Yilmaz, O. Wire Arc Additive Manufacturing of High-Strength Low Alloy Steels: Study of Process Parameters and Their Influence on the Bead Geometry and Mechanical Characteristics. *Int. J. Adv. Manuf. Technol.* **2020**, *108*, 3391–3404. [CrossRef]
26. Wang, H.; Jiang, W.; Ouyang, J.; Kovacevic, R. Rapid Prototyping of 4043 Al-Alloy Parts by VP-GTAW. *J. Mater. Process. Technol.* **2004**, *148*, 93–102. [CrossRef]
27. Dinovitzer, M.; Chen, X.; Laliberte, J.; Huang, X.; Frei, H. Effect of Wire and Arc Additive Manufacturing (WAAM) Process Parameters on Bead Geometry and Microstructure. *Addit. Manuf.* **2019**, *26*, 138–146. [CrossRef]
28. Wu, B.; Pan, Z.; Ding, D.; Cuiuri, D.; Li, H. Effects of Heat Accumulation on Microstructure and Mechanical Properties of Ti6Al4V Alloy Deposited by Wire Arc Additive Manufacturing. *Addit. Manuf.* **2018**, *23*, 151–160. [CrossRef]
29. Suryakumar, S.; Karunakaran, K.P.; Chandrasekhar, U.; Somashekara, M.A. A Study of the Mechanical Properties of Objects Built through Weld-Deposition. *Proc. Inst. Mech. Eng. Part B J. Eng. Manuf.* **2013**, *227*, 1138–1147. [CrossRef]
30. Oliveira, J.P.; Santos, T.G.; Miranda, R.M. Revisiting Fundamental Welding Concepts to Improve Additive Manufacturing: From Theory to Practice. *Prog. Mater. Sci.* **2020**, *107*, 100590. [CrossRef]
31. Pattanayak, S.; Sahoo, S.K. Gas Metal Arc Welding Based Additive Manufacturing—A Review. *CIRP J. Manuf. Sci. Technol.* **2021**, *33*, 398–442. [CrossRef]
32. Abe, T.; Kaneko, J.; Sasahara, H. Thermal Sensing and Heat Input Control for Thin-Walled Structure Building Based on Numerical Simulation for Wire and Arc Additive Manufacturing. *Addit. Manuf.* **2020**, *35*, 101357. [CrossRef]
33. Ouyang, J.H.; Wang, H.; Kovacevic, R. Rapid Prototyping of 5356-Aluminum Alloy Based on Variable Polarity Gas Tungsten Arc Welding: Process Control and Microstructure. *Mater. Manuf. Process.* **2002**, *17*, 103–124. [CrossRef]
34. Qi, K.; Li, R.; Hu, Z.; Bi, X.; Li, T.; Yue, H.; Zhang, B. Forming Appearance Analysis of 2205 Duplex Stainless Steel Fabricated by Cold Metal Transfer (CMT) Based Wire and Arc Additive Manufacture (WAAM) Process. *J. Mater. Eng. Perform.* **2022**, *31*, 4631–4641. [CrossRef]
35. Spencer, J.D.; Dickens, P.M.; Wykes, C.M. Rapid Prototyping of Metal Parts by Three-Dimensional Welding. *Proc. Inst. Mech. Eng. Part B J. Eng. Manuf.* **1998**, *212*, 175–182. [CrossRef]
36. da Silva, L.J.; Souza, D.M.; de Araújo, D.B.; Reis, R.P.; Scotti, A. Concept and Validation of an Active Cooling Technique to Mitigate Heat Accumulation in WAAM. *Int. J. Adv. Manuf. Technol.* **2020**, *107*, 2513–2523. [CrossRef]
37. Rodriguez, N.; Vázquez, L.; Huarte, I.; Arruti, E.; Tabernero, I.; Alvarez, P. Wire and Arc Additive Manufacturing: A Comparison between CMT and TopTIG Processes Applied to Stainless Steel. *Weld. World* **2018**, *62*, 1083–1096. [CrossRef]
38. Sames, W.J.; List, F.A.; Pannala, S.; Dehoff, R.R.; Babu, S.S. The Metallurgy and Processing Science of Metal Additive Manufacturing. *Int. Mater. Rev.* **2016**, *61*, 315–360. [CrossRef]

39. Wacker, C.; Köhler, M.; David, M.; Aschersleben, F.; Gabriel, F.; Hensel, J.; Dilger, K.; Dröder, K. Geometry and Distortion Prediction of Multiple Layers for Wire Arc Additive Manufacturing with Artificial Neural Networks. *Appl. Sci.* **2021**, *11*, 4694. [CrossRef]
40. Wu, B.; Pan, Z.; Ding, D.; Cuiuri, D.; Li, H.; Xu, J.; Norrish, J. A Review of the Wire Arc Additive Manufacturing of Metals: Properties, Defects and Quality Improvement. *J. Manuf. Process.* **2018**, *35*, 127–139. [CrossRef]
41. Ryan, E.M.; Sabin, T.J.; Watts, J.F.; Whiting, M.J. The Influence of Build Parameters and Wire Batch on Porosity of Wire and Arc Additive Manufactured Aluminium Alloy 2319. *J. Mater. Process. Technol.* **2018**, *262*, 577–584. [CrossRef]
42. Arana, M.; Ukar, E.; Rodriguez, I.; Iturrioz, A.; Alvarez, P. Strategies to Reduce Porosity in Al-Mg WAAM Parts and Their Impact on Mechanical Properties. *Metals* **2021**, *11*, 524. [CrossRef]
43. Gu, J.; Ding, J.; Williams, S.W.; Gu, H.; Ma, P.; Zhai, Y. The Effect of Inter-Layer Cold Working and Post-Deposition Heat Treatment on Porosity in Additively Manufactured Aluminum Alloys. *J. Mater. Process. Technol.* **2016**, *230*, 26–34. [CrossRef]
44. Hauser, T.; Reisch, R.T.; Breese, P.P.; Lutz, B.S.; Pantano, M.; Nalam, Y.; Bela, K.; Kamps, T.; Volpp, J.; Kaplan, A.F. Porosity in Wire Arc Additive Manufacturing of Aluminium Alloys. *Addit. Manuf.* **2021**, *41*, 101993. [CrossRef]
45. Fang, X.; Zhang, L.; Chen, G.; Dang, X.; Huang, K.; Wang, L.; Lu, B. Correlations between Microstructure Characteristics and Mechanical Properties in 5183 Aluminium Alloy Fabricated by Wire-Arc Additive Manufacturing with Different Arc Modes. *Materials* **2018**, *11*, 2075. [CrossRef] [PubMed]
46. Nguyen, T.C.; Weckman, D.C.; Johnson, D.A.; Kerr, H.W. High Speed Fusion Weld Bead Defects. *Sci. Technol. Weld. Join.* **2006**, *11*, 618–633. [CrossRef]
47. Xiong, J.; Zhang, G.; Gao, H.; Wu, L. Modeling of Bead Section Profile and Overlapping Beads with Experimental Validation for Robotic GMAW-Based Rapid Manufacturing. *Robot. Comput.-Integr. Manuf.* **2013**, *29*, 417–423. [CrossRef]
48. Gratzke, U.; Kapadia, P.D.; Dowden, J.; Kroos, J.; Simon, G. Theoretical Approach to the Humping Phenomenon in Welding Processes. *J. Phys. Appl. Phys.* **1992**, *25*, 1640. [CrossRef]
49. Belhadj, M.; Kromer, R.; Werda, S.; Darnis, P. Effect of Cold Metal Transfer-Based Wire Arc Additive Manufacturing Parameters on Geometry and Machining Allowance. *Res. Sq.* **2022**. [CrossRef]
50. Li, F.; Chen, S.; Shi, J.; Zhao, Y.; Tian, H. Thermoelectric Cooling-Aided Bead Geometry Regulation in Wire and Arc-Based Additive Manufacturing of Thin-Walled Structures. *Appl. Sci.* **2018**, *8*, 207. [CrossRef]
51. Wu, B.; Pan, Z.; Ding, D.; Cuiuri, D.; Li, H.; Fei, Z. The Effects of Forced Interpass Cooling on the Material Properties of Wire Arc Additively Manufactured Ti6Al4V Alloy. *J. Mater. Process. Technol.* **2018**, *258*, 97–105. [CrossRef]
52. Wang, L.; Xue, J.; Wang, Q. Correlation between Arc Mode, Microstructure, and Mechanical Properties during Wire Arc Additive Manufacturing of 316L Stainless Steel. *Mater. Sci. Eng. A* **2019**, *751*, 183–190. [CrossRef]
53. Stinson, H.; Ward, R.; Quinn, J.; McGarrigle, C. Comparison of Properties and Bead Geometry in MIG and CMT Single Layer Samples for WAAM Applications. *Metals* **2021**, *11*, 1530. [CrossRef]
54. Kumar, C.B.; Anandakrishnan, V. Experimental Investigations on the Effect of Wire Arc Additive Manufacturing Process Parameters on the Layer Geometry of Inconel 825. *Mater. Today Proc.* **2020**, *21*, 622–627. [CrossRef]
55. Sarathchandra, D.T.; Davidson, M.J.; Visvanathan, G. Parameters Effect on SS304 Beads Deposited by Wire Arc Additive Manufacturing. *Mater. Manuf. Process.* **2020**, *35*, 852–858. [CrossRef]
56. Lehmann, T.; Jain, A.; Jain, Y.; Stainer, H.; Wolfe, T.; Henein, H.; Qureshi, A.J. Concurrent Geometry-and Material-Based Process Identification and Optimization for Robotic CMT-Based Wire Arc Additive Manufacturing. *Mater. Des.* **2020**, *194*, 108841. [CrossRef]
57. Ding, D.; Pan, Z.; Cuiuri, D.; Li, H. A Multi-Bead Overlapping Model for Robotic Wire and Arc Additive Manufacturing (WAAM). *Robot. Comput.-Integr. Manuf.* **2015**, *31*, 101–110. [CrossRef]
58. Cunningham, C.R.; Flynn, J.M.; Shokrani, A.; Dhokia, V.; Newman, S.T. Invited Review Article: Strategies and Processes for High Quality Wire Arc Additive Manufacturing. *Addit. Manuf.* **2018**, *22*, 672–686. [CrossRef]
59. Kim, J.-D.; Kim, J.W.; Cheon, J.Y.; Kim, Y.-D.; Ji, C. Effect of Shielding Gases on the Wire Arc Additive Manufacturability of 5 Cr–4 Mo Tool Steel for Die Casting Mold Making. *Korean J. Met. Mater.* **2020**, *58*, 852–862. [CrossRef]
60. Gu, J.; Yang, S.; Gao, M.; Bai, J.; Zhai, Y.; Ding, J. Micropore Evolution in Additively Manufactured Aluminum Alloys under Heat Treatment and Inter-Layer Rolling. *Mater. Des.* **2020**, *186*, 108288. [CrossRef]
61. Li, Y.; Yu, S.; Chen, Y.; Yu, R.; Shi, Y. Wire and Arc Additive Manufacturing of Aluminum Alloy Lattice Structure. *J. Manuf. Process.* **2020**, *50*, 510–519. [CrossRef]
62. Zhao, Y.; Jia, Y.; Chen, S.; Shi, J.; Li, F. Process Planning Strategy for Wire-Arc Additive Manufacturing: Thermal Behavior Considerations. *Addit. Manuf.* **2020**, *32*, 100935. [CrossRef]
63. Zhu, L.; Luo, Y.; Han, J.; Zhang, C.; Xu, J.; Chen, D. Energy Characteristics of Droplet Transfer in Wire-Arc Additive Manufacturing Based on the Analysis of Arc Signals. *Measurement* **2019**, *134*, 804–813. [CrossRef]
64. Nie, Y.; Zhang, P.; Wu, X.; Li, G.; Yan, H.; Yu, Z. Rapid Prototyping of 4043 Al-Alloy Parts by Cold Metal Transfer. *Sci. Technol. Weld. Join.* **2018**, *23*, 527–535. [CrossRef]
65. Köhler, M.; Fiebig, S.; Hensel, J.; Dilger, K. Wire and Arc Additive Manufacturing of Aluminum Components. *Metals* **2019**, *9*, 608. [CrossRef]
66. Fang, X.; Li, H.; Li, X.; Huang, K.; Zhang, L.; Lu, B. Effect of Post Heat Treatment on the Microstructure and Mechanical Properties of Wire-Arc Additively Manufactured A357 Alloy Components. *Mater. Lett.* **2020**, *269*, 127674. [CrossRef]

67. Derekar, K.S.; Addison, A.; Joshi, S.S.; Zhang, X.; Lawrence, J.; Xu, L.; Melton, G.; Griffiths, D. Effect of Pulsed Metal Inert Gas (Pulsed-MIG) and Cold Metal Transfer (CMT) Techniques on Hydrogen Dissolution in Wire Arc Additive Manufacturing (WAAM) of Aluminium. *Int. J. Adv. Manuf. Technol.* **2020**, *107*, 311–331. [CrossRef]
68. Klein, T.; Schnall, M. Control of Macro-/Microstructure and Mechanical Properties of a Wire-Arc Additive Manufactured Aluminum Alloy. *Int. J. Adv. Manuf. Technol.* **2020**, *108*, 235–244. [CrossRef]
69. Li, S.; Zhang, L.-J.; Ning, J.; Wang, X.; Zhang, G.-F.; Zhang, J.-X.; Na, S.-J.; Fatemeh, B. Comparative Study on the Microstructures and Properties of Wire+ Arc Additively Manufactured 5356 Aluminium Alloy with Argon and Nitrogen as the Shielding Gas. *Addit. Manuf.* **2020**, *34*, 101206. [CrossRef]
70. Su, C.; Chen, X.; Gao, C.; Wang, Y. Effect of Heat Input on Microstructure and Mechanical Properties of Al-Mg Alloys Fabricated by WAAM. *Appl. Surf. Sci.* **2019**, *486*, 431–440. [CrossRef]
71. Baptista, R.J.S.; Pragana, J.P.M.; Bragança, I.M.F.; Silva, C.M.A.; Alves, L.M.; Martins, P.A.F. Joining Aluminium Profiles to Composite Sheets by Additive Manufacturing and Forming. *J. Mater. Process. Technol.* **2020**, *279*, 116587. [CrossRef]
72. Zhang, Z.; Sun, C.; Xu, X.; Liu, L. Surface Quality and Forming Characteristics of Thin-Wall Aluminium Alloy Parts Manufactured by Laser Assisted MIG Arc Additive Manufacturing. *Int. J. Lightweight Mater. Manuf.* **2018**, *1*, 89–95. [CrossRef]
73. Geng, H.; Li, J.; Xiong, J.; Lin, X. Optimisation of Interpass Temperature and Heat Input for Wire and Arc Additive Manufacturing 5A06 Aluminium Alloy. *Sci. Technol. Weld. Join.* **2017**, *22*, 472–483. [CrossRef]
74. Zhang, C.; Li, Y.; Gao, M.; Zeng, X. Wire Arc Additive Manufacturing of Al-6Mg Alloy Using Variable Polarity Cold Metal Transfer Arc as Power Source. *Mater. Sci. Eng. A* **2018**, *711*, 415–423. [CrossRef]
75. Gu, J.; Gao, M.; Yang, S.; Bai, J.; Zhai, Y.; Ding, J. Microstructure, Defects, and Mechanical Properties of Wire+ Arc Additively Manufactured AlCu4. 3-Mg1. 5 Alloy. *Mater. Des.* **2020**, *186*, 108357. [CrossRef]
76. Cadiou, S.; Courtois, M.; Carin, M.; Berckmans, W. 3D Heat Transfer, Fluid Flow and Electromagnetic Model for Cold Metal Transfer Wire Arc Additive Manufacturing (Cmt-Waam). *Addit. Manuf.* **2020**, *36*, 101541. [CrossRef]
77. Kumar, A.; Maji, K. Selection of Process Parameters for Near-Net Shape Deposition in Wire Arc Additive Manufacturing by Genetic Algorithm. *J. Mater. Eng. Perform.* **2020**, *29*, 3334–3352. [CrossRef]
78. Abe, T.; Mori, D.; Sonoya, K.; Nakamura, M.; Sasahara, H. Control of the Chemical Composition Distribution in Deposited Metal by Wire and Arc-Based Additive Manufacturing. *Precis. Eng.* **2019**, *55*, 231–239. [CrossRef]
79. Mai, D.S. Microstructural and Mechanical Characteristics of 308L Stainless Steel Manufactured by Gas Metal Arc Welding-Based Additive Manufacturing. *Mater. Lett.* **2020**, *271*, 127791.
80. Gordon, J.V.; Haden, C.V.; Nied, H.F.; Vinci, R.P.; Harlow, D.G. Fatigue Crack Growth Anisotropy, Texture and Residual Stress in Austenitic Steel Made by Wire and Arc Additive Manufacturing. *Mater. Sci. Eng. A* **2018**, *724*, 431–438. [CrossRef]
81. Abe, T.; Sasahara, H. Dissimilar Metal Deposition with a Stainless Steel and Nickel-Based Alloy Using Wire and Arc-Based Additive Manufacturing. *Precis. Eng.* **2016**, *45*, 387–395. [CrossRef]
82. Laghi, V.; Palermo, M.; Tonelli, L.; Gasparini, G.; Ceschini, L.; Trombetti, T. Tensile Properties and Microstructural Features of 304L Austenitic Stainless Steel Produced by Wire-and-Arc Additive Manufacturing. *Int. J. Adv. Manuf. Technol.* **2020**, *106*, 3693–3705. [CrossRef]
83. Haden, C.V.; Zeng, G.; Carter III, F.M.; Ruhl, C.; Krick, B.A.; Harlow, D.G. Wire and Arc Additive Manufactured Steel: Tensile and Wear Properties. *Addit. Manuf.* **2017**, *16*, 115–123. [CrossRef]
84. Shirizly, A.; Dolev, O. From Wire to Seamless Flow-Formed Tube: Leveraging the Combination of Wire Arc Additive Manufacturing and Metal Forming. *Jom* **2019**, *71*, 709–717. [CrossRef]
85. Lam, T.F.; Xiong, Y.; Dharmawan, A.G.; Foong, S.; Soh, G.S. Adaptive Process Control Implementation of Wire Arc Additive Manufacturing for Thin-Walled Components with Overhang Features. *Int. J. Adv. Manuf. Technol.* **2020**, *108*, 1061–1071. [CrossRef]
86. Chakkravarthy, V.; Jerome, S. Printability of Multiwalled SS 316L by Wire Arc Additive Manufacturing Route with Tunable Texture. *Mater. Lett.* **2020**, *260*, 126981. [CrossRef]
87. Wen, D.; Long, P.; Li, J.; Huang, L.; Zheng, Z. Effects of Linear Heat Input on Microstructure and Corrosion Behavior of an Austenitic Stainless Steel Processed by Wire Arc Additive Manufacturing. *Vacuum* **2020**, *173*, 109131. [CrossRef]
88. Ahsan, M.R.; Tanvir, A.N.M.; Seo, G.-J.; Bates, B.; Hawkins, W.; Lee, C.; Liaw, P.K.; Noakes, M.; Nycz, A.; Kim, D.B. Heat-Treatment Effects on a Bimetallic Additively-Manufactured Structure (BAMS) of the Low-Carbon Steel and Austenitic-Stainless Steel. *Addit. Manuf.* **2020**, *32*, 101036. [CrossRef]
89. Adinarayanappa, S.M.; Simhambhatla, S. Twin-Wire Welding Based Additive Manufacturing (TWAM): Manufacture of Functionally Gradient Objects. *Rapid Prototyp. J.* **2017**, *23*, 858–868. [CrossRef]
90. Rodrigues, T.A.; Duarte, V.R.; Tomás, D.; Avila, J.A.; Escobar, J.D.; Rossinyol, E.; Schell, N.; Santos, T.G.; Oliveira, J.P. In-Situ Strengthening of a High Strength Low Alloy Steel during Wire and Arc Additive Manufacturing (WAAM). *Addit. Manuf.* **2020**, *34*, 101200. [CrossRef]
91. Lu, X.; Zhou, Y.F.; Xing, X.L.; Shao, L.Y.; Yang, Q.X.; Gao, S.Y. Open-Source Wire and Arc Additive Manufacturing System: Formability, Microstructures, and Mechanical Properties. *Int. J. Adv. Manuf. Technol.* **2017**, *93*, 2145–2154. [CrossRef]
92. Hu, Z.; Qin, X.; Shao, T.; Liu, H. Understanding and Overcoming of Abnormity at Start and End of the Weld Bead in Additive Manufacturing with GMAW. *Int. J. Adv. Manuf. Technol.* **2018**, *95*, 2357–2368. [CrossRef]

93. Colegrove, P.A.; Coules, H.E.; Fairman, J.; Martina, F.; Kashoob, T.; Mamash, H.; Cozzolino, L.D. Microstructure and Residual Stress Improvement in Wire and Arc Additively Manufactured Parts through High-Pressure Rolling. *J. Mater. Process. Technol.* **2013**, *213*, 1782–1791. [CrossRef]
94. Yuan, L.; Pan, Z.; Ding, D.; Yu, Z.; van Duin, S.; Li, H.; Li, W.; Norrish, J. Fabrication of Metallic Parts with Overhanging Structures Using the Robotic Wire Arc Additive Manufacturing. *J. Manuf. Process.* **2021**, *63*, 24–34. [CrossRef]
95. Yuan, L.; Pan, Z.; Ding, D.; He, F.; van Duin, S.; Li, H.; Li, W. Investigation of Humping Phenomenon for the Multi-Directional Robotic Wire and Arc Additive Manufacturing. *Robot. Comput.-Integr. Manuf.* **2020**, *63*, 101916. [CrossRef]
96. Dirisu, P.; Supriyo, G.; Martina, F.; Xu, X.; Williams, S. Wire plus Arc Additive Manufactured Functional Steel Surfaces Enhanced by Rolling. *Int. J. Fatigue* **2020**, *130*, 105237. [CrossRef]
97. Cao, Y.; Zhu, S.; Liang, X.; Wang, W. Overlapping Model of Beads and Curve Fitting of Bead Section for Rapid Manufacturing by Robotic MAG Welding Process. *Robot. Comput.-Integr. Manuf.* **2011**, *27*, 641–645. [CrossRef]
98. Hackenhaar, W.; Mazzaferro, J.A.; Montevecchi, F.; Campatelli, G. An Experimental-Numerical Study of Active Cooling in Wire Arc Additive Manufacturing. *J. Manuf. Process.* **2020**, *52*, 58–65. [CrossRef]
99. Kozamernik, N.; Bračun, D.; Klobčar, D. WAAM System with Interpass Temperature Control and Forced Cooling for Near-Net-Shape Printing of Small Metal Components. *Int. J. Adv. Manuf. Technol.* **2020**, *110*, 1955–1968. [CrossRef]
100. Mohebbi, M.S.; Kühl, M.; Ploshikhin, V. A Thermo-Capillary-Gravity Model for Geometrical Analysis of Single-Bead Wire and Arc Additive Manufacturing (WAAM). *Int. J. Adv. Manuf. Technol.* **2020**, *109*, 877–891. [CrossRef]
101. Yang, D.; Wang, G.; Zhang, G. A Comparative Study of GMAW-and DE-GMAW-Based Additive Manufacturing Techniques: Thermal Behavior of the Deposition Process for Thin-Walled Parts. *Int. J. Adv. Manuf. Technol.* **2017**, *91*, 2175–2184. [CrossRef]
102. Li, Y.; Sun, Y.; Han, Q.; Zhang, G.; Horváth, I. Enhanced Beads Overlapping Model for Wire and Arc Additive Manufacturing of Multi-Layer Multi-Bead Metallic Parts. *J. Mater. Process. Technol.* **2018**, *252*, 838–848. [CrossRef]
103. Li, Y.; Han, Q.; Zhang, G.; Horváth, I. A Layers-Overlapping Strategy for Robotic Wire and Arc Additive Manufacturing of Multi-Layer Multi-Bead Components with Homogeneous Layers. *Int. J. Adv. Manuf. Technol.* **2018**, *96*, 3331–3344. [CrossRef]
104. Zhao, H.; Zhang, G.; Yin, Z.; Wu, L. A 3D Dynamic Analysis of Thermal Behavior during Single-Pass Multi-Layer Weld-Based Rapid Prototyping. *J. Mater. Process. Technol.* **2011**, *211*, 488–495. [CrossRef]
105. Li, Y.; Han, Q.; Horvath, I.; Zhang, G. Repairing Surface Defects of Metal Parts by Groove Machining and Wire+ Arc Based Filling. *J. Mater. Process. Technol.* **2019**, *274*, 116268. [CrossRef]
106. Li, Y.; Huang, X.; Horvath, I.; Zhang, G. GMAW-Based Additive Manufacturing of Inclined Multi-Layer Multi-Bead Parts with Flat-Position Deposition. *J. Mater. Process. Technol.* **2018**, *262*, 359–371. [CrossRef]
107. Xiong, J.; Zhang, G.; Qiu, Z.; Li, Y. Vision-Sensing and Bead Width Control of a Single-Bead Multi-Layer Part: Material and Energy Savings in GMAW-Based Rapid Manufacturing. *J. Clean. Prod.* **2013**, *41*, 82–88. [CrossRef]
108. Yang, D.; He, C.; Zhang, G. Forming Characteristics of Thin-Wall Steel Parts by Double Electrode GMAW Based Additive Manufacturing. *J. Mater. Process. Technol.* **2016**, *227*, 153–160. [CrossRef]
109. Xiong, J.; Yin, Z.; Zhang, W. Closed-Loop Control of Variable Layer Width for Thin-Walled Parts in Wire and Arc Additive Manufacturing. *J. Mater. Process. Technol.* **2016**, *233*, 100–106. [CrossRef]
110. Xiong, J.; Li, Y.; Li, R.; Yin, Z. Influences of Process Parameters on Surface Roughness of Multi-Layer Single-Pass Thin-Walled Parts in GMAW-Based Additive Manufacturing. *J. Mater. Process. Technol.* **2018**, *252*, 128–136. [CrossRef]
111. Li, Y.; Xiong, J.; Yin, Z. Molten Pool Stability of Thin-Wall Parts in Robotic GMA-Based Additive Manufacturing with Various Position Depositions. *Robot. Comput.-Integr. Manuf.* **2019**, *56*, 1–11. [CrossRef]
112. Xiong, J.; Liu, Y.; Yin, Z. Passive Vision Measurement for Robust Reconstruction of Molten Pool in Wire and Arc Additive Manufacturing. *Measurement* **2020**, *153*, 107407. [CrossRef]
113. Xiong, J.; Shi, M.; Liu, Y.; Yin, Z. Virtual Binocular Vision Sensing and Control of Molten Pool Width for Gas Metal Arc Additive Manufactured Thin-Walled Components. *Addit. Manuf.* **2020**, *33*, 101121. [CrossRef]
114. Li, Y.; Li, X.; Zhang, G.; Horváth, I.; Han, Q. Interlayer Closed-Loop Control of Forming Geometries for Wire and Arc Additive Manufacturing Based on Fuzzy-Logic Inference. *J. Manuf. Process.* **2021**, *63*, 35–47. [CrossRef]
115. Li, K.; Klecka, M.A.; Chen, S.; Xiong, W. Wire-Arc Additive Manufacturing and Post-Heat Treatment Optimization on Microstructure and Mechanical Properties of Grade 91 Steel. *Addit. Manuf.* **2021**, *37*, 101734. [CrossRef]
116. Ge, J.; Lin, J.; Chen, Y.; Lei, Y.; Fu, H. Characterization of Wire Arc Additive Manufacturing 2Cr13 Part: Process Stability, Microstructural Evolution, and Tensile Properties. *J. Alloys Compd.* **2018**, *748*, 911–921. [CrossRef]
117. Ge, J.; Lin, J.; Fu, H.; Lei, Y.; Xiao, R. A Spatial Periodicity of Microstructural Evolution and Anti-Indentation Properties of Wire-Arc Additive Manufacturing 2Cr13 Thin-Wall Part. *Mater. Des.* **2018**, *160*, 218–228. [CrossRef]
118. Kannan, A.R.; Shanmugam, N.S.; Rajkumar, V.; Vishnukumar, M. Insight into the Microstructural Features and Corrosion Properties of Wire Arc Additive Manufactured Super Duplex Stainless Steel (ER2594). *Mater. Lett.* **2020**, *270*, 127680. [CrossRef]
119. Ou, W.; Wei, Y.; Liu, R.; Zhao, W.; Cai, J. Determination of the Control Points for Circle and Triangle Route in Wire Arc Additive Manufacturing (WAAM). *J. Manuf. Process.* **2020**, *53*, 84–98. [CrossRef]
120. Ou, W.; Mukherjee, T.; Knapp, G.L.; Wei, Y.; DebRoy, T. Fusion Zone Geometries, Cooling Rates and Solidification Parameters during Wire Arc Additive Manufacturing. *Int. J. Heat Mass Transf.* **2018**, *127*, 1084–1094. [CrossRef]
121. Youheng, F.; Guilan, W.; Haiou, Z.; Liye, L. Optimization of Surface Appearance for Wire and Arc Additive Manufacturing of Bainite Steel. *Int. J. Adv. Manuf. Technol.* **2017**, *91*, 301–313. [CrossRef]

122. Marenych, O.O.; Kostryzhev, A.G.; Pan, Z.; Li, H.; van Duin, S. Comparative Effect of Mn/Ti Solute Atoms and TiC/Ni3 (Al, Ti) Nano-Particles on Work Hardening Behaviour in NiCu Alloys Fabricated by Wire Arc Additive Manufacturing. *Mater. Sci. Eng. A* **2019**, *753*, 262–275. [CrossRef]
123. Yin, X.; He, G.; Meng, W.; Xu, Z.; Hu, L.; Ma, Q. Comparison Study of Low-Heat-Input Wire Arc-Fabricated Nickel-Based Alloy by Cold Metal Transfer and Plasma Arc. *J. Mater. Eng. Perform.* **2020**, *29*, 4222–4232. [CrossRef]
124. Jurić, I.; Garašić, I.; Bušić, M.; Kožuh, Z. Influence of Shielding Gas Composition on Structure and Mechanical Properties of Wire and Arc Additive Manufactured Inconel 625. *Jom* **2019**, *71*, 703–708. [CrossRef]
125. Yangfan, W.; Xizhang, C.; Chuanchu, S. Microstructure and Mechanical Properties of Inconel 625 Fabricated by Wire-Arc Additive Manufacturing. *Surf. Coat. Technol.* **2019**, *374*, 116–123. [CrossRef]
126. Tian, Y.; Ouyang, B.; Gontcharov, A.; Gauvin, R.; Lowden, P.; Brochu, M. Microstructure Evolution of Inconel 625 with 0.4 Wt% Boron Modification during Gas Tungsten Arc Deposition. *J. Alloys Compd.* **2017**, *694*, 429–438. [CrossRef]
127. Van, D.; Dinda, G.P.; Park, J.; Mazumder, J.; Lee, S.H. Enhancing Hardness of Inconel 718 Deposits Using the Aging Effects of Cold Metal Transfer-Based Additive Manufacturing. *Mater. Sci. Eng. A* **2020**, *776*, 139005. [CrossRef]
128. Gou, J.; Wang, Z.; Hu, S.; Shen, J.; Tian, Y.; Zhao, G.; Chen, Y. Effects of Ultrasonic Peening Treatment in Three Directions on Grain Refinement and Anisotropy of Cold Metal Transfer Additive Manufactured Ti-6Al-4V Thin Wall Structure. *J. Manuf. Process.* **2020**, *54*, 148–157. [CrossRef]
129. Ding, D.; Wu, B.; Pan, Z.; Qiu, Z.; Li, H. Wire Arc Additive Manufacturing of Ti6AL4V Using Active Interpass Cooling. *Mater. Manuf. Process.* **2020**, *35*, 845–851. [CrossRef]
130. Gou, J.; Wang, Z.; Hu, S.; Shen, J.; Tian, Y.; Zhao, G.; Chen, Y. Effects of Trace Nb Addition on Microstructure and Properties of Ti–6Al–4V Thin-Wall Structure Prepared via Cold Metal Transfer Additive Manufacturing. *J. Alloys Compd.* **2020**, *829*, 154481. [CrossRef]
131. Bambach, M.; Sizova, I.; Sydow, B.; Hemes, S.; Meiners, F. Hybrid Manufacturing of Components from Ti-6Al-4V by Metal Forming and Wire-Arc Additive Manufacturing. *J. Mater. Process. Technol.* **2020**, *282*, 116689. [CrossRef]
132. Li, Z.; Liu, C.; Xu, T.; Ji, L.; Wang, D.; Lu, J.; Ma, S.; Fan, H. Reducing Arc Heat Input and Obtaining Equiaxed Grains by Hot-Wire Method during Arc Additive Manufacturing Titanium Alloy. *Mater. Sci. Eng. A* **2019**, *742*, 287–294. [CrossRef]
133. Ng, C.H.; Bermingham, M.J.; Kent, D.; Dargusch, M.S. High Stability and High Strength β-Titanium Alloys for Additive Manufacturing. *Mater. Sci. Eng. A* **2021**, *816*, 141326. [CrossRef]
134. Guo, Y.; Quan, G.; Celikin, M.; Ren, L.; Zhan, Y.; Fan, L.; Pan, H. Effect of Heat Treatment on the Microstructure and Mechanical Properties of AZ80M Magnesium Alloy Fabricated by Wire Arc Additive Manufacturing. *J. Magnes. Alloys* **2021**, *10*, 1930–1940. [CrossRef]
135. Yang, X.; Liu, J.; Wang, Z.; Lin, X.; Liu, F.; Huang, W.; Liang, E. Microstructure and Mechanical Properties of Wire and Arc Additive Manufactured AZ31 Magnesium Alloy Using Cold Metal Transfer Process. *Mater. Sci. Eng. A* **2020**, *774*, 138942. [CrossRef]
136. Yuan, T.; Luo, Z.; Kou, S. Grain Refining of Magnesium Welds by Arc Oscillation. *Acta Mater.* **2016**, *116*, 166–176. [CrossRef]
137. Deshmukh, P.S.; Tomar, K.; Sathiaraj, G.D.; Palani, I.A. Optimum Strength and Ductility of Pure Copper Fabricated by Wire Arc Additive Manufacturing. *Manuf. Lett.* **2022**, *33*, 24–28. [CrossRef]
138. Baby, J.; Amirthalingam, M. Microstructural Development during Wire Arc Additive Manufacturing of Copper-Based Components. *Weld. World* **2020**, *64*, 395–405. [CrossRef]
139. Chen, W.; Chen, Y.; Zhang, T.; Wen, T.; Feng, X.; Yin, L. Effects of Location on the Microstructure and Mechanical Properties of Cu-8Al-2Ni-2Fe-2Mn Alloy Produced Through Wire Arc Additive Manufacturing. *J. Mater. Eng. Perform.* **2020**, *29*, 4733–4744. [CrossRef]
140. Rodrigues, T.A.; Bairrão, N.; Farias, F.W.C.; Shamsolhodaei, A.; Shen, J.; Zhou, N.; Maawad, E.; Schell, N.; Santos, T.G.; Oliveira, J.P. Steel-Copper Functionally Graded Material Produced by Twin-Wire and Arc Additive Manufacturing (T-WAAM). *Mater. Des.* **2022**, *213*, 110270. [CrossRef]
141. Wang, Y.; Konovalov, S.; Chen, X.; Ivanov, Y.; Jayalakshmi, S.; Singh, R.A. Research on Cu-6.6% Al-3.2% Si Alloy by Dual Wire Arc Additive Manufacturing. *J. Mater. Eng. Perform.* **2021**, *30*, 1694–1702. [CrossRef]
142. Wang, Y.; Chen, X.; Konovalov, S.; Su, C.; Siddiquee, A.N.; Gangil, N. In-Situ Wire-Feed Additive Manufacturing of Cu-Al Alloy by Addition of Silicon. *Appl. Surf. Sci.* **2019**, *487*, 1366–1375. [CrossRef]
143. Oražem, Ž. Vpliv Medvarkovne Temperature Pri Oblikovnem Obločnem Navarjanju Brona CuAl8. Bachelor's Thesis, University of Ljubljana, Ljubljana, Slovenia, 2019.
144. Lin, Z.; Ya, W.; Subramanian, V.V.; Goulas, C.; di Castri, B.; Hermans, M.J.; Pathiraj, B. Deposition of Stellite 6 Alloy on Steel Substrates Using Wire and Arc Additive Manufacturing. *Int. J. Adv. Manuf. Technol.* **2020**, *111*, 411–426. [CrossRef]
145. Zhang, S.; Zhang, Y.; Gao, M.; Wang, F.; Li, Q.; Zeng, X. Effects of Milling Thickness on Wire Deposition Accuracy of Hybrid Additive/Subtractive Manufacturing. *Sci. Technol. Weld. Join.* **2019**, *24*, 375–381. [CrossRef]
146. Duarte, V.R.; Rodrigues, T.A.; Schell, N.; Miranda, R.M.; Oliveira, J.P.; Santos, T.G. Hot Forging Wire and Arc Additive Manufacturing (HF-WAAM). *Addit. Manuf.* **2020**, *35*, 101193. [CrossRef]
147. Shi, J.; Li, F.; Chen, S.; Zhao, Y.; Tian, H. Effect of In-Process Active Cooling on Forming Quality and Efficiency of Tandem GMAW–Based Additive Manufacturing. *Int. J. Adv. Manuf. Technol.* **2019**, *101*, 1349–1356. [CrossRef]
148. Hackenhaar, W.; Montevecchi, F.; Scippa, A.; Campatelli, G. Air-Cooling Influence on Wire Arc Additive Manufactured Surfaces. In *Key Engineering Materials*; Trans Tech Publications Ltd.: Wollerau, Switzerland, 2019; Volume 813, pp. 241–247.
149. Nagamatsu, H.; Sasahara, H.; Mitsutake, Y.; Hamamoto, T. Development of a Cooperative System for Wire and Arc Additive Manufacturing and Machining. *Addit. Manuf.* **2020**, *31*, 100896. [CrossRef]

150. Xia, C.; Pan, Z.; Polden, J.; Li, H.; Xu, Y.; Chen, S.; Zhang, Y. A Review on Wire Arc Additive Manufacturing: Monitoring, Control and a Framework of Automated System. *J. Manuf. Syst.* **2020**, *57*, 31–45. [CrossRef]
151. Tang, F.; Luo, Y.; Cai, Y.; Yang, S.; Zhang, F.; Peng, Y. Arc Length Identification Based on Arc Acoustic Signals in GTA-WAAM Process. *Int. J. Adv. Manuf. Technol.* **2022**, *118*, 1553–1563. [CrossRef]
152. Chabot, A.; Rauch, M.; Hascoët, J.-Y. Novel Control Model of Contact-Tip-to-Work Distance (CTWD) for Sound Monitoring of Arc-Based DED Processes Based on Spectral Analysis. *Int. J. Adv. Manuf. Technol.* **2021**, *116*, 3463–3472. [CrossRef]
153. Pal, K.; Bhattacharya, S.; Pal, S.K. Investigation on Arc Sound and Metal Transfer Modes for On-Line Monitoring in Pulsed Gas Metal Arc Welding. *J. Mater. Process. Technol.* **2010**, *210*, 1397–1410. [CrossRef]
154. Pal, K.; Bhattacharya, S.; Pal, S.K. Prediction of Metal Deposition from Arc Sound and Weld Temperature Signatures in Pulsed MIG Welding. *Int. J. Adv. Manuf. Technol.* **2009**, *45*, 1113–1130. [CrossRef]
155. Zhan, Q.; Liang, Y.; Ding, J.; Williams, S. A Wire Deflection Detection Method Based on Image Processing in Wire+ Arc Additive Manufacturing. *Int. J. Adv. Manuf. Technol.* **2017**, *89*, 755–763. [CrossRef]
156. Hallam, J.M.; Kissinger, T.; Charrett, T.O.; Tatam, R.P. In-Process Range-Resolved Interferometric (RRI) 3d Layer Height Measurements for Wire+ Arc Additive Manufacturing (WAAM). *Meas. Sci. Technol.* **2022**, *33*, 044002. [CrossRef]
157. Xiong, J.; Zhang, Y.; Pi, Y. Control of Deposition Height in WAAM Using Visual Inspection of Previous and Current Layers. *J. Intell. Manuf.* **2021**, *32*, 2209–2217. [CrossRef]
158. Halisch, C.; Radel, T.; Tyralla, D.; Seefeld, T. Measuring the Melt Pool Size in a Wire Arc Additive Manufacturing Process Using a High Dynamic Range Two-Colored Pyrometric Camera. *Weld. World* **2020**, *64*, 1349–1356. [CrossRef]
159. Shen, H.; Lin, T.; Chen, S.; Li, L. Real-Time Seam Tracking Technology of Welding Robot with Visual Sensing. *J. Intell. Robot. Syst.* **2010**, *59*, 283–298. [CrossRef]
160. Xu, Y.; Fang, G.; Chen, S.; Zou, J.J.; Ye, Z. Real-Time Image Processing for Vision-Based Weld Seam Tracking in Robotic GMAW. *Int. J. Adv. Manuf. Technol.* **2014**, *73*, 1413–1425. [CrossRef]
161. Jorge, V.L.; Teixeira, F.R.; Scotti, A. Pyrometrical Interlayer Temperature Measurement in WAAM of Thin Wall: Strategies, Limitations and Functionality. *Metals* **2022**, *12*, 765. [CrossRef]
162. Shi, M.; Xiong, J.; Zhang, G.; Zheng, S. Monitoring Process Stability in GTA Additive Manufacturing Based on Vision Sensing of Arc Length. *Measurement* **2021**, *185*, 110001. [CrossRef]
163. Bonaccorso, F.; Cantelli, L.; Muscato, G. An Arc Welding Robot Control for a Shaped Metal Deposition Plant: Modular Software Interface and Sensors. *IEEE Trans. Ind. Electron.* **2011**, *58*, 3126–3132. [CrossRef]
164. Xiong, J.; Zhang, G. Online Measurement of Bead Geometry in GMAW-Based Additive Manufacturing Using Passive Vision. *Meas. Sci. Technol.* **2013**, *24*, 115103. [CrossRef]
165. Baier, D.; Wolf, F.; Weckenmann, T.; Lehmann, M.; Zaeh, M.F. Thermal Process Monitoring and Control for a Near-Net-Shape Wire and Arc Additive Manufacturing. *Prod. Eng.* **2022**, *16*, 811–822. [CrossRef]
166. da Silva, L.J.; Reis, R.P.; Scotti, A. The Potential of IR Pyrometry for Monitoring Interpass Temperature in Wire+ Arc Additive Manufacturing. *Evol. Mech. Eng.* **2019**, *3*, 1–4. [CrossRef]
167. Veiga, F.; Suarez, A.; Aldalur, E.; Artaza, T. Wire Arc Additive Manufacturing of Invar Parts: Bead Geometry and Melt Pool Monitoring. *Measurement* **2022**, *189*, 110452. [CrossRef]
168. Cunha, F.G.; Santos, T.G.; Xavier, J. In Situ Monitoring of Wire and Arc Additive Manufacturing by Digital Image Correlation: A Case Study. *Procedia Struct. Integr.* **2022**, *37*, 33–40. [CrossRef]
169. Sreedhar, U.; Krishnamurthy, C.V.; Balasubramaniam, K.; Raghupathy, V.D.; Ravisankar, S. Automatic Defect Identification Using Thermal Image Analysis for Online Weld Quality Monitoring. *J. Mater. Process. Technol.* **2012**, *212*, 1557–1566. [CrossRef]
170. Zhang, Z.; Yu, H.; Lv, N.; Chen, S. Real-Time Defect Detection in Pulsed GTAW of Al Alloys through on-Line Spectroscopy. *J. Mater. Process. Technol.* **2013**, *213*, 1146–1156. [CrossRef]
171. Huang, Y.; Wu, D.; Zhang, Z.; Chen, H.; Chen, S. EMD-Based Pulsed TIG Welding Process Porosity Defect Detection and Defect Diagnosis Using GA-SVM. *J. Mater. Process. Technol.* **2017**, *239*, 92–102. [CrossRef]
172. Zhang, C.; Gao, M.; Chen, C.; Zeng, X. Spectral Diagnosis of Wire Arc Additive Manufacturing of Al Alloys. *Addit. Manuf.* **2019**, *30*, 100869. [CrossRef]
173. Xiong, J.; Yu, Y.; Zheng, S.; Zhang, G. Arc Voltage Measurements for Height Control in Pulsed Arc Additive Manufacturing. *Measurement* **2022**, *191*, 110867. [CrossRef]
174. Jin, P.; Liu, Y.; Sun, Q. Evolution of Crystallographic Orientation, Columnar to Equiaxed Transformation and Mechanical Properties Realized by Adding TiCps in Wire and Arc Additive Manufacturing 2219 Aluminum Alloy. *Addit. Manuf.* **2021**, *39*, 101878. [CrossRef]
175. Gu, J.; Yang, S.; Gao, M.; Bai, J.; Liu, K. Influence of Deposition Strategy of Structural Interface on Microstructures and Mechanical Properties of Additively Manufactured Al Alloy. *Addit. Manuf.* **2020**, *34*, 101370. [CrossRef]
176. Gomez Ortega, A.; Corona Galvan, L.; Deschaux-Beaume, F.; Mezrag, B.; Rouquette, S. Effect of Process Parameters on the Quality of Aluminium Alloy Al5Si Deposits in Wire and Arc Additive Manufacturing Using a Cold Metal Transfer Process. *Sci. Technol. Weld. Join.* **2018**, *23*, 316–332. [CrossRef]
177. Luo, Y.; Li, J.; Xu, J.; Zhu, L.; Han, J.; Zhang, C. Influence of Pulsed Arc on the Metal Droplet Deposited by Projected Transfer Mode in Wire-Arc Additive Manufacturing. *J. Mater. Process. Technol.* **2018**, *259*, 353–360. [CrossRef]

178. Yuan, T.; Yu, Z.; Chen, S.; Xu, M.; Jiang, X. Loss of Elemental Mg during Wire+ Arc Additive Manufacturing of Al-Mg Alloy and Its Effect on Mechanical Properties. *J. Manuf. Process.* **2020**, *49*, 456–462. [CrossRef]
179. Horgar, A.; Fostervoll, H.; Nyhus, B.; Ren, X.; Eriksson, M.; Akselsen, O.M. Additive Manufacturing Using WAAM with AA5183 Wire. *J. Mater. Process. Technol.* **2018**, *259*, 68–74. [CrossRef]
180. Feng, Y.; Zhan, B.; He, J.; Wang, K. The Double-Wire Feed and Plasma Arc Additive Manufacturing Process for Deposition in Cr-Ni Stainless Steel. *J. Mater. Process. Technol.* **2018**, *259*, 206–215. [CrossRef]
181. Nilsiam, Y.; Sanders, P.G.; Pearce, J.M. Applications of Open Source GMAW-Based Metal 3-D Printing. *J. Manuf. Mater. Process.* **2018**, *2*, 18. [CrossRef]
182. Kapil, S.; Legesse, F.; Kulkarni, P.; Joshi, P.; Desai, A.; Karunakaran, K.P. Hybrid-Layered Manufacturing Using Tungsten Inert Gas Cladding. *Prog. Addit. Manuf.* **2016**, *1*, 79–91. [CrossRef]
183. Mai, D.S.; Paris, H. Influences of the Compressed Dry Air-Based Active Cooling on External and Internal Qualities of Wire-Arc Additive Manufactured Thin-Walled SS308L Components. *J. Manuf. Process.* **2021**, *62*, 18–27.
184. Suárez, A.; Aldalur, E.; Veiga, F.; Artaza, T.; Tabernero, I.; Lamikiz, A. Wire Arc Additive Manufacturing of an Aeronautic Fitting with Different Metal Alloys: From the Design to the Part. *J. Manuf. Process.* **2021**, *64*, 188–197. [CrossRef]
185. Wang, Y.; Chen, X.; Shen, Q.; Su, C.; Zhang, Y.; Jayalakshmi, S.; Singh, R.A. Effect of Magnetic Field on the Microstructure and Mechanical Properties of Inconel 625 Superalloy Fabricated by Wire Arc Additive Manufacturing. *J. Manuf. Process.* **2021**, *64*, 10–19. [CrossRef]
186. Xu, F.; Lv, Y.; Liu, Y.; Shu, F.; He, P.; Xu, B. Microstructural Evolution and Mechanical Properties of Inconel 625 Alloy during Pulsed Plasma Arc Deposition Process. *J. Mater. Sci. Technol.* **2013**, *29*, 480–488. [CrossRef]
187. Lin, J.; Lv, Y.; Liu, Y.; Sun, Z.; Wang, K.; Li, Z.; Wu, Y.; Xu, B. Microstructural Evolution and Mechanical Property of Ti-6Al-4V Wall Deposited by Continuous Plasma Arc Additive Manufacturing without Post Heat Treatment. *J. Mech. Behav. Biomed. Mater.* **2017**, *69*, 19–29. [CrossRef]
188. Bermingham, M.J.; Thomson-Larkins, J.; St John, D.H.; Dargusch, M.S. Sensitivity of Ti-6Al-4V Components to Oxidation during out of Chamber Wire+ Arc Additive Manufacturing. *J. Mater. Process. Technol.* **2018**, *258*, 29–37. [CrossRef]
189. Martina, F.; Roy, M.J.; Szost, B.A.; Terzi, S.; Colegrove, P.A.; Williams, S.W.; Withers, P.J.; Meyer, J.; Hofmann, M. Residual Stress of As-Deposited and Rolled Wire+ Arc Additive Manufacturing Ti–6Al–4V Components. *Mater. Sci. Technol.* **2016**, *32*, 1439–1448. [CrossRef]
190. Baufeld, B.; Van der Biest, O. Mechanical Properties of Ti-6Al-4V Specimens Produced by Shaped Metal Deposition. *Sci. Technol. Adv. Mater.* **2009**, *10*, 015008. [CrossRef]
191. Donoghue, J.; Antonysamy, A.A.; Martina, F.; Colegrove, P.A.; Williams, S.W.; Prangnell, P.B. The Effectiveness of Combining Rolling Deformation with Wire–Arc Additive Manufacture on β-Grain Refinement and Texture Modification in Ti–6Al–4V. *Mater. Charact.* **2016**, *114*, 103–114. [CrossRef]
192. Kennedy, J.R.; Davis, A.E.; Caballero, A.E.; White, M.; Fellowes, J.; Pickering, E.J.; Prangnell, P.B. Microstructure Transition Gradients in Titanium Dissimilar Alloy (Ti-5Al-5V-5Mo-3Cr/Ti-6Al-4V) Tailored Wire-Arc Additively Manufactured Components. *Mater. Charact.* **2021**, *182*, 111577. [CrossRef]
193. Guo, Y.; Pan, H.; Ren, L.; Quan, G. Microstructure and Mechanical Properties of Wire Arc Additively Manufactured AZ80M Magnesium Alloy. *Mater. Lett.* **2019**, *247*, 4–6. [CrossRef]
194. Guo, J.; Zhou, Y.; Liu, C.; Wu, Q.; Chen, X.; Lu, J. Wire Arc Additive Manufacturing of AZ31 Magnesium Alloy: Grain Refinement by Adjusting Pulse Frequency. *Materials* **2016**, *9*, 823. [CrossRef] [PubMed]
195. Wang, P.; Zhang, H.; Zhu, H.; Li, Q.; Feng, M. Wire-Arc Additive Manufacturing of AZ31 Magnesium Alloy Fabricated by Cold Metal Transfer Heat Source: Processing, Microstructure, and Mechanical Behavior. *J. Mater. Process. Technol.* **2021**, *288*, 116895. [CrossRef]
196. Li, J.; Qiu, Y.; Yang, J.; Sheng, Y.; Yi, Y.; Zeng, X.; Chen, L.; Yin, F.; Su, J.; Zhang, T.; et al. Effect of Grain Refinement Induced by Wire and Arc Additive Manufacture (WAAM) on the Corrosion Behaviors of AZ31 Magnesium Alloy in NaCl Solution. *J. Magnes. Alloys* **2021**, *11*. [CrossRef]
197. Chen, W.; Chen, Y.; Zhang, T.; Wen, T.; Yin, Z.; Feng, X. Effect of Ultrasonic Vibration and Interpass Temperature on Microstructure and Mechanical Properties of Cu-8Al-2Ni-2Fe-2Mn Alloy Fabricated by Wire Arc Additive Manufacturing. *Metals* **2020**, *10*, 215. [CrossRef]
198. Queguineur, A.; Rückert, G.; Cortial, F.; Hascoët, J.Y. Evaluation of Wire Arc Additive Manufacturing for Large-Sized Components in Naval Applications. *Weld. World* **2018**, *62*, 259–266. [CrossRef]
199. Taheri, H.; Shoaib, M.R.B.M.; Koester, L.W.; Bigelow, T.A.; Collins, P.C.; Bond, L.J. Powder-Based Additive Manufacturing-a Review of Types of Defects, Generation Mechanisms, Detection, Property Evaluation and Metrology. *Int. J. Addit. Subtractive Mater. Manuf.* **2017**, *1*, 172–209. [CrossRef]
200. Hauser, T.; Reisch, R.T.; Seebauer, S.; Parasar, A.; Kamps, T.; Casati, R.; Volpp, J.; Kaplan, A.F. Multi-Material Wire Arc Additive Manufacturing of Low and High Alloyed Aluminium Alloys with in-Situ Material Analysis. *J. Manuf. Process.* **2021**, *69*, 378–390. [CrossRef]
201. Mohan Kumar, S.; Rajesh Kannan, A.; Pravin Kumar, N.; Pramod, R.; Siva Shanmugam, N.; Vishnu, A.S.; Channabasavanna, S.G. Microstructural Features and Mechanical Integrity of Wire Arc Additive Manufactured SS321/Inconel 625 Functionally Gradient Material. *J. Mater. Eng. Perform.* **2021**, *30*, 5692–5703. [CrossRef]

202. Ahsan, M.R.U.; Tanvir, A.N.M.; Ross, T.; Elsawy, A.; Oh, M.-S.; Kim, D.B. Fabrication of Bimetallic Additively Manufactured Structure (BAMS) of Low Carbon Steel and 316L Austenitic Stainless Steel with Wire+ Arc Additive Manufacturing. *Rapid Prototyp. J.* **2020**, *26*, 519–530. [CrossRef]
203. Deutsches Kupferinstitut. Low-Alloyed Copper Alloys. Available online: https://kupfer.de/wp-content/uploads/2019/11/RZ_Niedriglegierte_Kupferwerkstoffe_i8_EN_Einzelseiten.pdf (accessed on 5 August 2022).
204. KOBE STEEL, Ltd. Site Search—Arc Welding OfNonferrous Metals. Available online: https://search.kobelco.co.jp/search?site=EJ4JC91U&design=2&charset=UTF-8&group=4&query=Arc+Welding+ofNonferrous+Metals&x=28&y=8&pdf=27 (accessed on 5 August 2022).
205. Hybird Resources. Copper Alloy Wire Archives. Available online: https://hybirdresources.com/products/copper-product/copper-alloy-wire (accessed on 5 August 2022).
206. DRATEC Drahttechnik GmbH. Copper. Available online: https://dratec.de/ (accessed on 5 August 2022).
207. Williams, S.W.; Pardal, A.R.G.; Quintino, L.; de Tecnologia Mecanica, S. Wire And Arc Additive Manufacture of Highly Conducting Pure Copper. In Proceedings of the RAPDASA 2019 Conference Proceedings, Bloemfontein, South Africa, 6–8 November 2019; Volume 1, pp. 1–4.
208. Dong, B.; Pan, Z.; Shen, C.; Ma, Y.; Li, H. Fabrication of Copper-Rich Cu-Al Alloy Using the Wire-Arc Additive Manufacturing Process. *Metall. Mater. Trans. B* **2017**, *48*, 3143–3151. [CrossRef]

Disclaimer/Publisher's Note: The statements, opinions and data contained in all publications are solely those of the individual author(s) and contributor(s) and not of MDPI and/or the editor(s). MDPI and/or the editor(s) disclaim responsibility for any injury to people or property resulting from any ideas, methods, instructions or products referred to in the content.